Thermal Science and Engineering Progress 39 (2023) 101734

Contents lists available at ScienceDirect

Thermal Science and Engineering Progress

journal homepage: www.sciencedirect.com/journal/thermal-science-and-engineering-progress

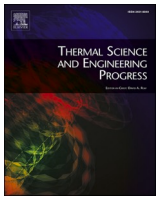

The influence of splitter blades and meridional profiles on the performance of small-scale turbopumps for ORC applications; analysis, neural network modeling and optimization

Sajjad Zakeralhoseini *, Jürg Schiffmann

Ecole Polytechnique Fédérale de Lausanne (EPFL), Laboratory for Applied Mechanical Design, CH-1015 Lausanne, Switzerland

ARTICLE INFO

Keywords:
Turbopumps
ORC
Splitter blades
Meridional profiles
CFD
Optimization

ABSTRACT

This work presents the influence of splitters on the performance of small-scale turbopumps for organic Rankine cycle applications numerically. Different design parameters, such as impeller diameter at the outlet, number of blades, blade angle at the trailing edge, and the length and location of the splitter blades, are studied for both shrouded and unshrouded impellers at tip clearance ratios of 0.05 and 0.10 (relative to blade height). The results suggest that splitter blades can increase impeller head coefficient and slip factors up to 10%–24% depending on the blade outlet angle. At the same time, the total efficiency is not influenced significantly. The CFD calculations predict that the placement of splitters in the middle of the blade channel leads to the maximum head coefficient for shrouded impellers. In contrast, for the tip clearance ratio of 0.10, a higher head coefficient is observed for placement closer to the suction side of the main blade. After that, different meridional profiles are studied to investigate their influence on the performance characteristics and mitigation of tip clearance effects. Profiles with a sharper change of cross-section area at the inlet rather than a linear change are found more advantageous, as higher head rise, total efficiency, and static efficiency are observed. In the end, the splitter blade profiles are optimized through techniques of design of experiments, leading to a 2.43% improvement in total efficiency. In contrast, the head rise remains constant, and static efficiency decreases by 0.49% for an impeller with a tip clearance ratio of 0.05.

Introduction

The organic Rankine cycle (ORC) system [1] is among the technologies that have been applied to exploit the waste heat of exhaust gases. The working principle of the ORC is very similar to the Rankine cycle. The significant difference lies in the working fluid: The ORC works with organic fluids characterized by higher molecular weights and lower boiling pressure than water [2]. Since common organic fluids have lower latent heat than water, higher mass flow rates are required to convert the same amount of waste heat, which considerably increases the pump size and energy usage. The weight and size of standard pumps can significantly penalize the benefits of installing waste heat recovery on vehicles. Hence, efficient and more compact pumps, such as small-scale turbopumps, would be very welcome for mobile waste heat recovery applications. Typically, a turbopump design is achieved through mean-line calculations and empirical correlations derived from existing designs. However, a turbopump's performance is also affected by additional parameters such as splitter blade and tip clearance, which models in the literature do not systematically address, particularly not at the scales required for ORC in waste heat recovery, as highlighted below.

Splitter blades

Gölcü et al. [3] reported an efficiency improvement of 1.14% using splitter blades for impellers with five blades. They showed that the splitter blades negatively influenced the efficiency of pumps with 6 and 7 blades. Kergourlay et al. [4] showed that the splitter blades negatively affect the pump efficiency while the pressure rise increases due to an increase in the slip coefficient. Zhou et al. [5] presented a method for the design of low specific-speed pumps with splitter blades based on 2-d flow analysis. Their findings revealed that the leading edge of splitter blades has a significant impact on performance. Shigemitsu et al. [6] suggested that conventional design theory does not apply to small-sized machines. They showed that the splitter blades decrease the low-

* Corresponding author.
E-mail addresses: sajjad.zakeralhoseini@epfl.ch (S. Zakeralhoseini), jurg.schiffmann@epfl.ch (J. Schiffmann).

https://doi.org/10.1016/j.tsep.2023.101734
Received 27 October 2022; Received in revised form 13 February 2023; Accepted 15 February 2023
Available online 23 February 2023
2451-9049/© 2023 The Author(s). Published by Elsevier Ltd. This is an open access article under the CC BY license (http://creativecommons.org/licenses/by/4.0/).

Nomenclature

b	blade height, m
c	clearance gap, m
c	absolute velocity, m s^{-1}
H	head, m
m	meridional length, m
Q	flow rate, m^3 s^{-1}
r	radius, m
u	peripheral velocity, m s^{-1}
w	relative velocity, m s^{-1}
Z	number of blades
z	axial length
p_s	static pressure, Pa
$p_{T,r}$	reduced stagnation pressure, Pa
C_p	pressure coefficient
n_q	specific speed, rpm, m^3 s^{-1}, m, $\frac{nQ^{1/2}}{H^{3/4}}$
n_s	specific speed, non-dimensional, $n_q/52.9$

Greek letters

β	flow angle, °
β_B	blade angle, °
ρ	density, kg m-3
γ	slip factor
ω	rotational speed, rad s^{-1}
ψ	head coefficient, $\frac{gH}{\omega^2 r_2^2}$
η	efficiency

Subscripts

i	inlet
h	hub
le	leading edge
m	meridional component
mb	main blades
o	outlet
PS	pressure side
s	shroud
sp	splitter blades
SS	suction side
u	circumferential component
0	shrouded impeller
1	inlet station
2	outlet station
∞	blade congruent flow

Abbreviations

CFD	computational fluid dynamics
DOE	design of experiment
GA	genetic algorithm
NN	neural network
NSGA	non-dominated sorting genetic algorithm
RSM	response surface method
ORC	organic Rankine cycle
OSFD	optimal-space filling design
SST	shear stress transport

velocity regions throughout the blade channel, improving small-sized centrifugal pumps' performance.

Cavazzini et al. [7] suggested that the splitter blades improve the non-cavitating operating range of the pump at relatively high mass flow rates, while the suction performance is depreciated at low flow rates. This conclusion is consistent with the results presented by Yang et al. [8]. They showed that the required suction pressure is reduced because the blade loading is distributed between the main and splitter blades, which increases the pump's efficiency notably at high flow rates. Yuan [9] showed that the splitter blades smoothen the jet-wake pattern and decrease the flow separations from the main blade, increasing the pump's efficiency by 4%. Zhang et al. [10] argued that the secondary flows and flow circulation on the main blade pressure side are mitigated when the trailing edge of the splitter blades is closer to the main blade suction side. Yuan et al. [11] proposed a correlation giving the trailing edge diameter of splitter blades for low-specific speed centrifugal pumps based on the inlet and outlet diameters of the impeller. They claimed that placing splitter blades closer to the suction side of the adjacent main blades could improve the flow pattern and performance.

Djebedjian [12] revised the slip factor proposed by Wiesner [13] to predict the performance characteristics of centrifugal pumps equipped with splitters. Zhang et al. [14] developed an artificial neural network model based on 85 groups of experimental data for predicting the head coefficient and efficiency of centrifugal pumps with splitter blades. Le et al. [15] reported a flattened head-flow curve with an increment between 2% and 12% in head rise due to the addition of splitters to centrifugal pumps. Siddique et al. [16] showed that the splitter blade can improve the head rise and efficiency by 8.2% and 3% at the best efficiency point. They concluded that such improvement is induced by the uniform blade loading achieved with splitter blades.

The literature review on splitter blades in turbopumps reveals studies for shrouded impellers or specific pump designs. Though the researchers are divided on the benefits of adding splitter blades to the pump's efficiency, some suggest that they may improve the pump's head rise. Unfortunately, the combined effects of splitter blades and tip clearance for a wide range of specific speeds and design parameters have not been considered. Further, the conducted studies are limited to splitter blades generated from the rotation and cutting of the main blade. Using a proper optimization method, it may be possible to shape splitter blades differently from the main blades to improve a particular performance indicator of a pump, such as decreasing the required inlet pressure or increasing the head rise.

Design optimization

The pump's efficiency can be improved by implementing optimization techniques to determine optimized geometrical parameters. Optimization methods based on function approximation techniques, such as neural networks (NN) and response surfaces, have been successfully implemented in the design methodology of turbopump components [17]. Lian and Liou [18] achieved an increase of 1.8% in stage pressure ratio and a decrease of 5.4% in weight by optimizing the meridional geometry and blade angles. Kim et al. [19] used the combination of Design of Experiment (DOE) and RSM techniques to find the optimized geometrical parameters of the impeller and the diffuser of a mixed-flow pump. Huang et al. [20] optimized the blade loading of a centrifugal impeller using GA and NN by varying ten parameters on the blade profiles for given meridional profiles. An optimized solution providing smoother velocity gradients on the suction side without flow separation at the inlet was obtained as a result of the optimization.

Pei et al. [21] optimized the meridional parameters of a centrifugal impeller based on DOE, RSM, and GA techniques. The meridional profiles were parametrized with the arc radii and angles of the hub and shroud profiles. Compared to the baseline design, a 6.1% increase in total efficiency at the design flow rate was achieved. Pei et al. [22] investigated the influence of the inlet diameter, blade incidence angle, and blade wrap angle on the cavitation characteristics of a centrifugal pump using DOE and RSM techniques based on CFD analyses. They

successfully achieved a design providing higher hydraulic and cavitation performance, as the required suction head decreased by 0.63 m compared to the baseline impeller. Suh et al. [23] optimized the impeller and diffuser of a second-stage multi-phase pump using DOE and surrogate models based on RSM techniques. Compared to the baseline design, a 1.1% increase in total efficiency and a 3.1% increase in the static efficiency of the diffuser were reported.

Namazizadeh et al. [24] optimized the head rise and efficiency of a centrifugal pump by varying the splitter blade location in the impeller blade span and its leading-edge position using the design of experiments and response surface methods. An increase of 4.4% in the head rise compared to the initial splitter blade geometry is achieved with the optimization process. Approximately a 15% increment in the head rise is observed compared to the base impeller without splitter blades.

To the best of the authors' knowledge, the influence of splitter blade geometrical parameters and their ideal design for shrouded and unshrouded impellers have not yet been thoroughly researched in the literature. The cost-effective investigation of splitter blade effects is made possible by the development of accurate numerical methods and robust computational resources. The CFD analysis can be employed to optimize geometrical parameters and profiles, which are not addressed by reduced-order models and would be expensive to do through experiments.

In this paper, the influence of the governing parameters of splitter blades on the performance of small-scale turbopumps is investigated through CFD analyses. The variations of the slip factor, head rise, and efficiency with influential parameters are evaluated. The CFD results are then utilized to infer reduced-order models that will be used in the preliminary design and optimization of such machines. The models enable engineers to dimension a new turbopump with fewer iterations for ORC applications. The study is followed by optimizing the meridional profiles and the shape of splitter blades to increase the impeller's head rise and total efficiency.

Methodology

Several centrifugal impellers should be investigated to appropriately cover the design space to analyze the effect of different geometrical parameters on the turbopump performance. Thoroughly studying the impact of these multiple parameters through CFD is possible only if an automated tool is available for generating different geometries. Therefore, a parametric design tool is developed to generate different centrifugal impeller designs analyzed through CFD. The CFD analysis includes creating the fluid domain, generating the grid, defining the physics, equations, and boundary conditions, finally solving the problem, and post-process the data to extract the performance indicators and flow patterns. Given that several geometries will be examined, the CFD process must also be steered by the parametric design tool. Wide-ranging turbopump geometries are generated with the parametric design model for their assessment with a CFD solver. Fig. 1 presents the methodology of this work.

The authors developed the modeling tool and design methodology as presented in [25,26]. For the given main dimensions of an impeller, such as inlet and outlet radii, the hub and shroud profiles are necessary to create a three-dimensional geometry of the impeller. The developed procedure is based on the medial axis theory [27,28] in which the meridional shapes are built systematically for a given medial axis (see Fig. 2), making it a proficient method for the automated generation of different profiles.

The coordinates of the medial axis (r, z) can are established based on a statistical model as described in [26]. The medial axis curve can be achieved by solving the following equations:

$$z(s) = \int_0^s \frac{dz}{ds} ds = \int_0^s \cos\alpha(s) ds$$

$$r(s) = d_0/2 + \int_0^s \frac{dr}{ds} ds = r_0 + \int_0^s \sin\alpha(s) ds \quad (1)$$

where s is the tangential coordinate along the curve, and α is its angle with the z-axis in a counterclockwise direction (see Fig. 2). Zou et al. [42] suggested that the medial axis curve for a centrifugal pump can consist of five segments, with endpoints determined with Eq. (2):

$$S_1 = 0$$

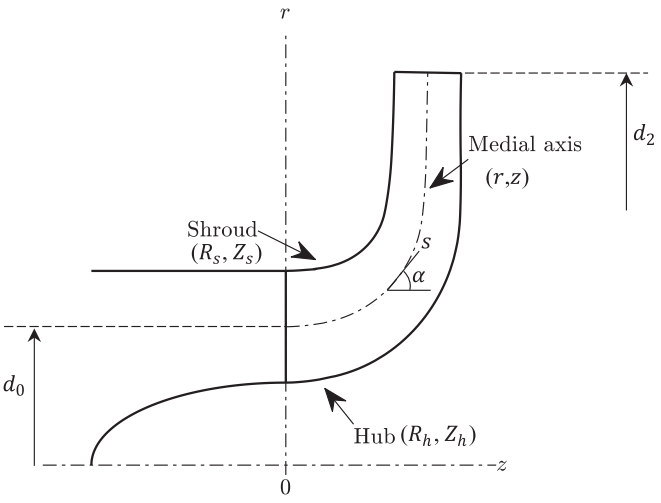

Fig. 2. Meridional profiles: hub, shroud, and medial axis.

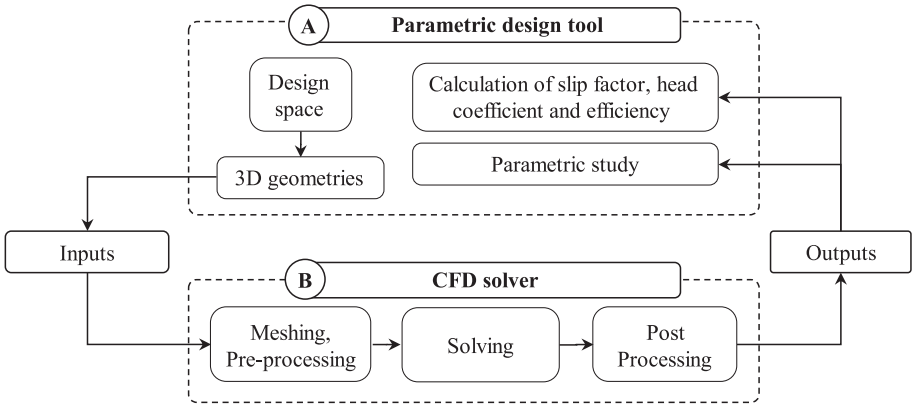

Fig. 1. Methodology flowchart.

$$S_2 = -0.2697e^{-8.748n_s} + 0.1377$$

$$S_3 = -0.5791e^{-2.429n_s} + 0.7477$$

$$S_4 = -0.6175e^{-2.466n_s} + 0.7852$$

$$S_5 = -0.5614e^{-2.544n_s} + 0.9160$$

$$S_6 = 1 \tag{2}$$

where $S = s/L$ is the endpoints of the segment normalized with the medial axis length (L). For each segment, the tangent (α) was suggested to be:

$$\alpha_1 = 0$$

$$\alpha_2 = -2.1e^{-26.63n_s} + 0.2092$$

$$\alpha_3 = 1.424$$

$$\alpha_4 = 1.467$$

$$\alpha_5 = 1.552$$

$$\alpha_5 = \alpha_6 \tag{3}$$

Then, the coordinates of the hub (R_h, Z_h) and shroud (R_s, Z_s) profiles can be calculated for the given medial axis and the given distribution of the cross-section area from the inlet to the outlet ($F(r)$). The distribution function ($F(r)$) relates the coordinates of the medial axis, hub, and shrouded as follows:

$$F(r) = \frac{4}{9}\pi(R_s + R_h + r)\left\{\sqrt{[Z_s - z(r)]^2 + [R_s - r]^2} + \sqrt{[Z_s - Z_h]^2 + [R_s - R_h]^2}\right\} \tag{4}$$

In addition, the $F(r)$ function relates the change of the meridional component of the relative velocity to the coordinates of the hub and shroud profiles. The profiles are generated with a linear distribution of the cross-section area. The procedure of solving the mathematical formulation to compute the four coordinate variables of hub and shroud profiles (R_s, Z_s, R_h and Z_h) is based on a constrained optimization problem which is detailed in [25]. Eq. (5) defines the objective function of the minimization problem. The equation combines two equations (C_1 and C_2) governing the coordinates of hub (R_h, Z_h) and shroud (R_s, Z_s) with respect to the achieved medial axis (r, z):

$$C(R_s, R_h, Z_s, Z_h) = |C_1| + |C_2| \tag{5}$$

$$C_1 = F(r) - \frac{4}{9}\pi(r + R_h + R_s) \times \left\{\sqrt{(Z_s - z)^2 + (R_s - r)^2} + \sqrt{(Z_s - Z_h)^2 + (R_s - R_h)^2}\right\} \tag{6}$$

$$C_2 = \frac{Z_s + Z_h}{2} - z\left(\frac{R_s + R_h}{2}\right) \tag{7}$$

The constraints of the minimization problem are given in Eq. (8) to Eq (10):

$$Z_h = \frac{\{R_s - R_h + 2z(r)z'(r) + (R_s + R_h - 2r)[z'(r)]^2\}}{2z'(r)} \tag{8}$$

$$Z_s = \frac{\{R_h - R_s + 2z(r)z'(r) + (R_s + R_h - 2r)[z'(r)]^2\}}{2z'(r)} \tag{9}$$

$$z \le \frac{Z_s + Z_h}{2} \tag{10}$$

The following step shapes the blade profiles. The blade is shaped in three dimensions at the leading edge and is tapered to a two-dimensional shape at the trailing edge. A blade shape can be defined by (1) a blade angle distribution and (2) a blade thickness distribution. The blade angle is distributed with two equal-length parabolic curves with a common tangent at the intersection, satisfying the imposed blade angles at the leading and trailing edges. The blade angle function can be written as follows (see Fig. 3):

$$\begin{cases} f_1(m) = a_1m^2 + b_1m + c_1m \le m_t \\ f_2(m) = a_2m^2 + b_2m + c_2m > m_t \end{cases} \tag{11}$$

where m_t is the common tangent point, which is equal to half of the total meridional length.

The blade angle development with two parabolic curves results in a system of six equations:

$$\begin{cases} f_1'(m_t) = f_2'(m_t) \\ f_1'(m_{le}) = 0 \\ f_2'(0) = 0 \\ f_1(m_t) = f_2(m_t) \\ f_1(m_{le}) = \beta_1 \\ f_2(0) = \beta_2 \end{cases} \tag{12}$$

The unknown coefficients can then be determined using the Gauss-elimination algorithm. The developed blade profile represents the camber-line of a blade section, which can then be dimensioned with a thickness function of $t = t(m)$. For each camber-line, the leading edge is shaped elliptically. The elliptic leading edge's semi-major axis (a) is five times the blade thickness (see Fig. 4). The thickness function for the elliptic section can be written as follows:

$$t = (b/a)\sqrt{a^2 - m^2} \tag{13}$$

Then the thickness of the blade gradually decreases toward the trailing edge to half of its maximum thickness to reduce the pressure fluctuations.

The tool automatically generates turbopump geometries within the parametric ranges listed in Table 1, leading to 1620 impellers assessed with CFD. The parameters satisfy the requirements of small-scale waste heat recovery systems based on ORC, specifically a system with a net output power of 8 kW for truck engines and running with R245fa as a working fluid [29,30]. The corresponding turbopump should deliver a head rise of 155 m and a flow of 0.768 m^3/h at the design point.

The splitter blades are created by rotating the main blades along the axis of rotation and trimming their leading edge at a certain meridional

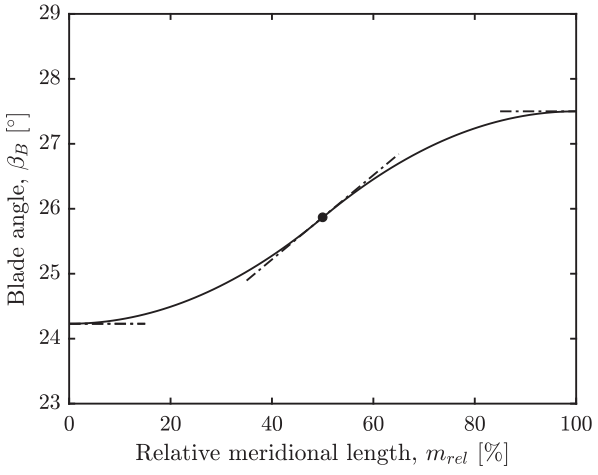

Fig. 3. An example of blade angle development with two parabolic curves.

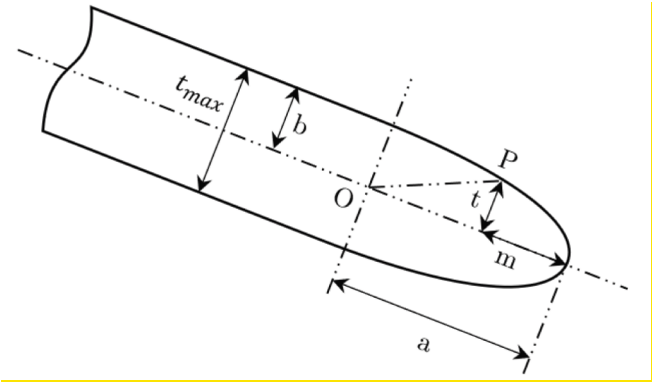

Fig. 4. Elliptic profile of the leading edge.

Table 1
Parameter ranges of ORC turbopumps.

Parameter	Symbol	Range	Unit
Blade angle	β_B	22.5, 50, 90	(°)
No. blades	Z	4, 5, 6	(–)
Tip clearance ratio	c/b	shrouded, 0.05, 0.1	(%)
Rotational speed	n	40, 50, 75	(krpm)
Pitch of splitter blades	φ_{sp}	25, 37, 50, 62, 75	(%)
Relative meridional location of splitter blades	$m'_{le,sp}$	12, 25, 40, 55	(%)

length, as depicted in Fig. 5. Therefore, the blade angle and thickness of splitters are the same as the main blades in each radius. The pitch of splitter blades determines the angular location of splitters relative to the main blades in the blade channel and is calculated as follows:

$$\varphi_{sp} = \frac{\theta_{sp}}{\theta_{mb}} \tag{14}$$

where θ_{sp} is the angle between the splitter blade and the adjacent pressure side of the main blade and θ_{mb} is the angle between two adjacent blades. Hence, a low φ_{sp} characterizes a splitter blade close to the pressure side and a large one close to the suction side of the main blade. The relative leading-edge location of the splitter blades is determined by dividing the meridional location of the leading edge of splitters ($m_{le,sp}$) to the total meridional length of the main blade (m_{mb}):

$$m'_{le,sp} = \frac{m_{le,sp}}{m_{mb}} \tag{15}$$

A low $m'_{le,sp}$ characterizes a splitter blade close to a full blade, while a large value represents a very short splitter blade. The computational domain consists of an inlet pipe followed by the impeller. Only one blade channel is simulated to reduce the computational cost. ANSYS TurboGrid [31] is employed to generate the mesh of the computational domain. The impeller grid is structured to ensure a proper resolution of the boundary layers. The global size factor of the grid is set to 1.20. The grid specification near the walls of the blades, hub, and shroud is governed by a target y^+ and the Reynolds number based on the blade chord length. The topology is established by control points placed on different layers from the hub to the shroud. The grid is finer around the blades to capture its complex geometry and to obtain sufficiently low y^+ values. A finer grid is also generated in the tip clearance of unshrouded impellers (at least 45 layers with an end ratio of 30). The grid specifications are chosen based on a mesh independence study for impellers with blade outlet angles of 22.5°, 50°, and 90°. The 3-d analysis is carried out for meshes with different global size factors for three impellers. Fig. 6 presents the pressure rise (relative to selected grid values) of three impellers at different global size factors. The figure suggests that at a size factor of around 1.10, the pressure rise begins to plateau. Therefore, a global size factor of 1.20, which ensures mesh-independent results while keeping the computation resources reasonable, is chosen.

ANSYS CFX is employed for the viscous 3D analysis of the pump flows. The investigation is carried out for R245fa in a liquid state with density and dynamic viscosity of 1311.9 kg.m^{-3} and 3.525 × 10^{-4} Pa.s, respectively. The turbulence is modeled with the shear stress transport (SST) method [38]. The advection terms and turbulence equations are discretized with a high-resolution scheme. The domain of volume flowing in the inlet pipe is set to stationary. A rotational reference

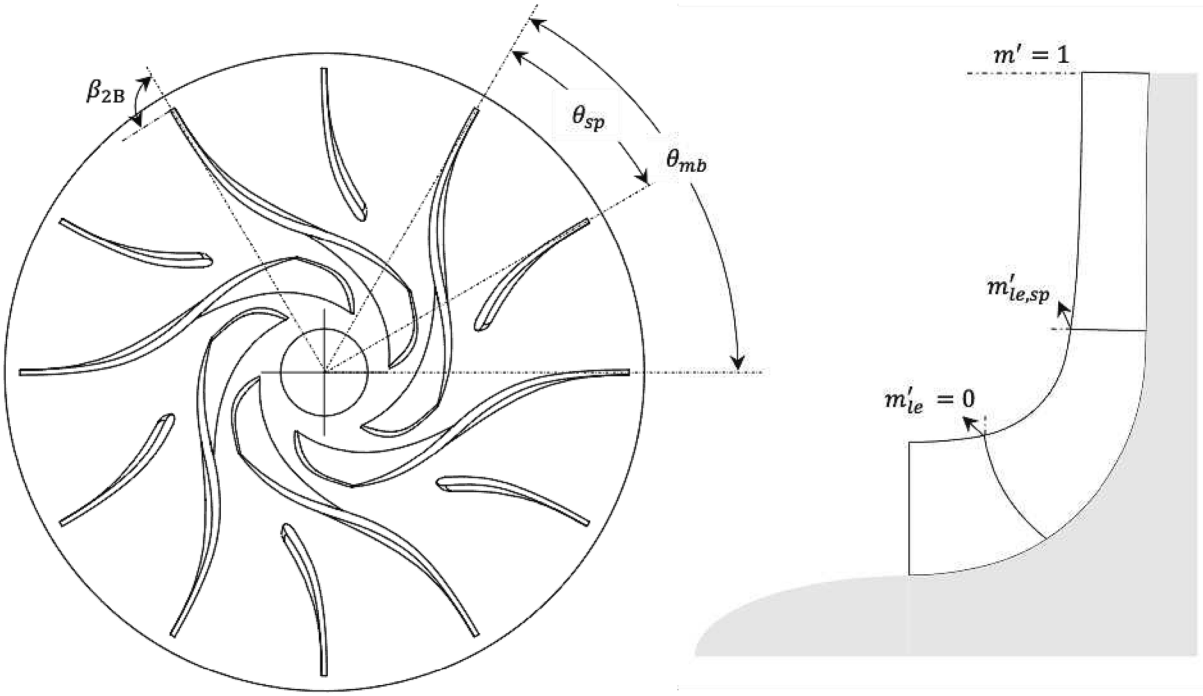

Fig. 5. Splitter blade parameters.

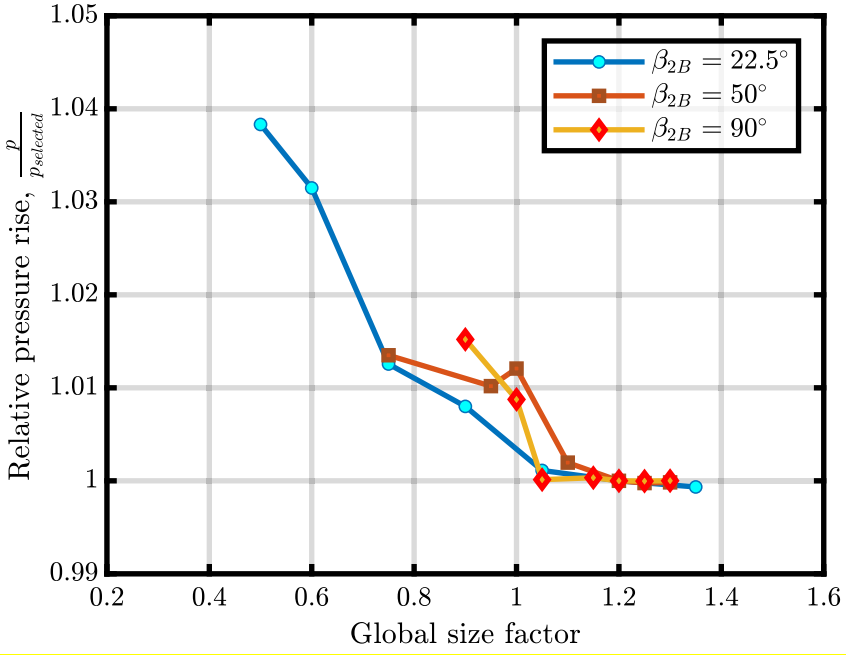

Fig. 6. Grids independence study for two studied turbopumps.

coordinate system is considered on the volume circulating in the impeller around the axis of the pump. The total pressure at the pipe inlet and the mass flow rate at the impeller outlet are set as boundary conditions. The walls are treated as no-slip walls. The steady-state analysis is performed to visualize the influence of design parameters on the pump's performance cost-efficiently. The analyses are carried out at the duty flow rate with the maximum residual convergence criteria set to 10^{-5}. The developed tool shown in Fig. 1 propagates the problem to six workstations running on Intel Xeon Processor E5-1650 v3 3.50 GHz.

Results and discussion

The results obtained from the numerical approach enable the characterization of performance indicators, such as slip factor, efficiency, and head coefficient as a function of geometric variables.

Methodology validation

The methodology can be validated by comparing the slip factor calculated from the CFD results with the predictions of well-known correlations. The slip factor can be defined with Eq. (16):

$$\gamma = 1 - \frac{c_{u2\infty} - c_{u2}}{u_2} \tag{16}$$

where $c_{u2\infty}$ is the circumferential component of absolute velocity for an impeller with an infinite number of blades. Fig. 7 summarizes the relative deviations of slip factors predicted by correlations compared to CFD data for all shrouded impellers without splitters. Relative error (e_i) and mean relative errors ($\bar{e}$) as well as standard deviation (σ) defined by Eq. (17) to Eq. (19), respectively, are considered for the evaluation of the different correlations:

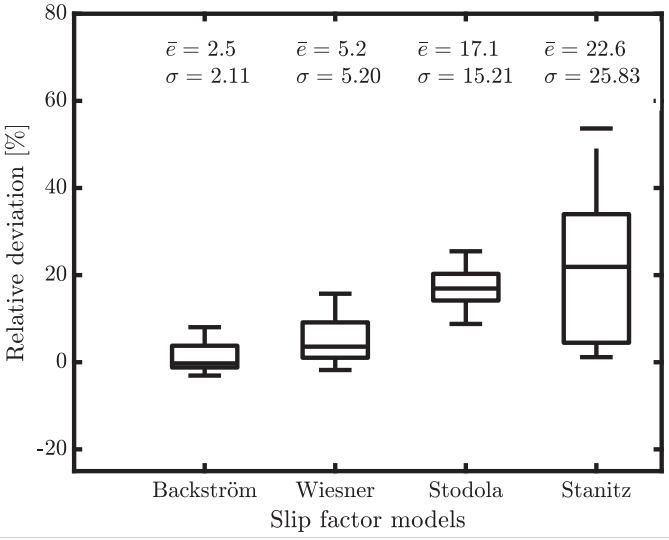

Fig. 7. Relative deviation of slip factors predicted with correlations compared to CFD data for all shrouded impellers without splitters.

$$e_i = \frac{X_{predicted_i} - X_{CFDi}}{X_{CFDi}} \times 100 \quad (17)$$

$$\bar{e} = \frac{1}{n}\sum_1^n e_i \quad (18)$$

$$\sigma = \sqrt{\frac{1}{n}\sum_1^n (e_i - \bar{e})^2} \quad (19)$$

The correlations of Von Backström [39] and Wiesner [13] predict 100% and 90.1% of the slip factors within a relative error of ±10%. Only 2% and 60% of the predictions with the correlations of Stodola [40] and Stanitz [41] are within 10% relative deviation. The very good agreement between the CFD results for shrouded impellers without splitters and the well-known correlations of Von Backström [39] and Wiesner [13] validates the reliability of the CFD analysis carried out on the turbopump geometries.

Performance analysis

Shrouded impellers

Fig. 8 presents the relative head coefficient for the different values of splitters' pitch and length for shrouded impellers with 5 blades and a blade outlet angle of 22.5°. The head coefficients are plotted relative to the corresponding impeller without splitters (0.1496 at the design flow rate). CFD calculations do not converge for splitters with a relative leading-edge location of 12% at high pitch values of 62.5% and 75%. The calculations might fail due to the high-order discretization scheme used for the equations, which can lead to instabilities for complex meshes of impellers with long splitter blades. The figure suggests that by employing splitter blades, the head rise is increased by up to 18%. The optimal pitch of the splitters with a relative leading-edge location of 12% and 25% is in the middle of the adjacent main blades ($\varphi_{sp} = 0.5$). For shorter splitters, the optimal splitters move toward the pressure side of the adjacent main blades leading to a pitch between 37% and 50%.

In other words, Fig. 8 suggests that at low pitch values, i.e., when the splitters are closer to the pressure side, the head rise increment is more pronounced for shorter splitters. The slip factor can elucidate this observation since it considers the influence of flow deviation from the path imposed by the blades in decreasing energy transmission.

In Fig. 9, the slip factors (relative to the impeller without splitters, $\gamma_{wosp} = 0.8202$) are computed and shown for the same impellers presented in Fig. 8.

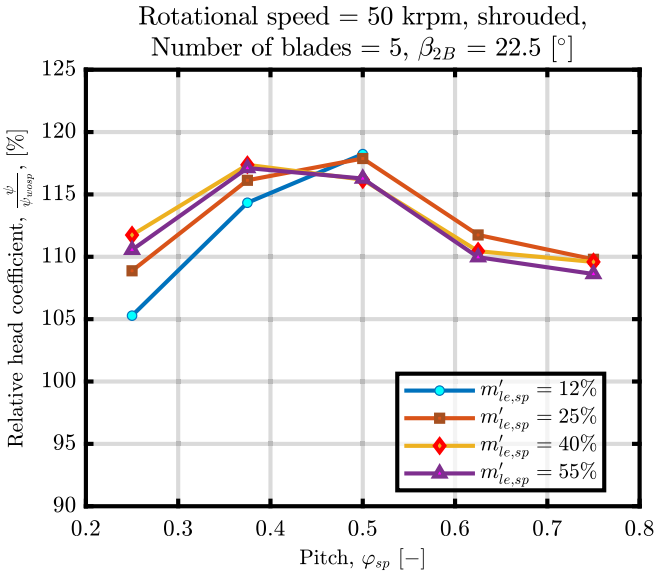

Fig. 8. The effects of pitch and length of splitter blades on the head coefficient.

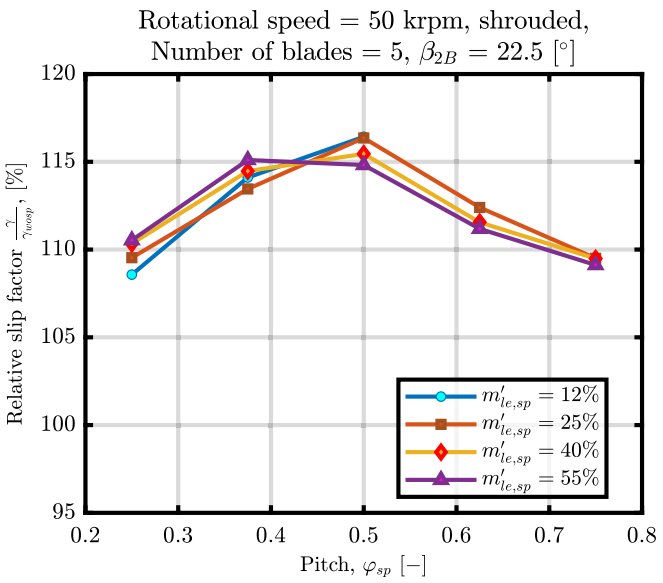

Fig. 9. The effects of pitch and length of splitter blades on the slip factor.

The curves suggest that the increment of slip factor for long splitters ($m'_{le,sp}$ = 12 % and 25 %) at a low pitch is relatively smaller, which indicates a more significant flow deviation, probably due to wake and jet flows caused by the interference of the splitters with the main flow. Such observation can be made clear by visualizing flow contours at the trailing edge section of the impeller. Fig. 10 presents the contour of normalized velocity (w/u_2) at the trailing edge section. It suggests the formation of a wake zone (indicated by blue) between the pressure side of the main blade and the adjacent splitter blade for long splitters on the one hand ($m'_{le,sp}$ = 12 % and 25 %). On the other hand, the flow is accelerated more between the splitter's pressure side and the main blade's suction side. Such non-uniformity of the flow for long splitters causes the mixed-out circumferential component of absolute velocity (c_{u2}) to drop (see Fig. 11). Referring to Euler's equation of turbomachinery [32] and the slip factor definition of Eq. (16), the head rise of a pump relies significantly on the circumferential component of absolute velocity (c_{u2}). Therefore, as the c_{u2} is smaller for long splitters, the head coefficient and slip factor diminish.

In Fig. 12, the relative total efficiency ($\eta_{t,wosp}$ = 95.4 %) is plotted at different pitches and lengths of splitter blades for shrouded impellers. The total efficiency is computed by dividing the given useful power by the shaft power as follows:

$$\eta = 100 \times \frac{\rho Q g H_{in\ to\ out}}{P_{shaft}} \quad (20)$$

Fig. 12 reveals that the splitter blades barely influence the total efficiency, as the efficiency increase is less than 1 %. Referring to the previous figures, the performance indicators generally depend less on the length of the splitter blades. Yuan and Yuan [9] reported a similar observation through an experimental study. In addition, referring to slip factor and flow vectors, lower efficiency is expected for long splitters at low pitches, as seen in Fig. 12.

Fig. 13 presents the influence of the pitch and length of splitter blades on the relative static efficiency ($\eta_{s,wosp}$ = 66.5 %) for shrouded impellers. The static efficiency is the ratio of the power difference attributed to the static head at the outlet and the power attributed to the total head at the inlet to the shaft power as follows:

$$\eta = 100 \times \frac{\rho Q g (H_{s,o} - H_{t,in})}{P_{shaft}} \quad (21)$$

The figure suggests that the static efficiency reaches a minimum at

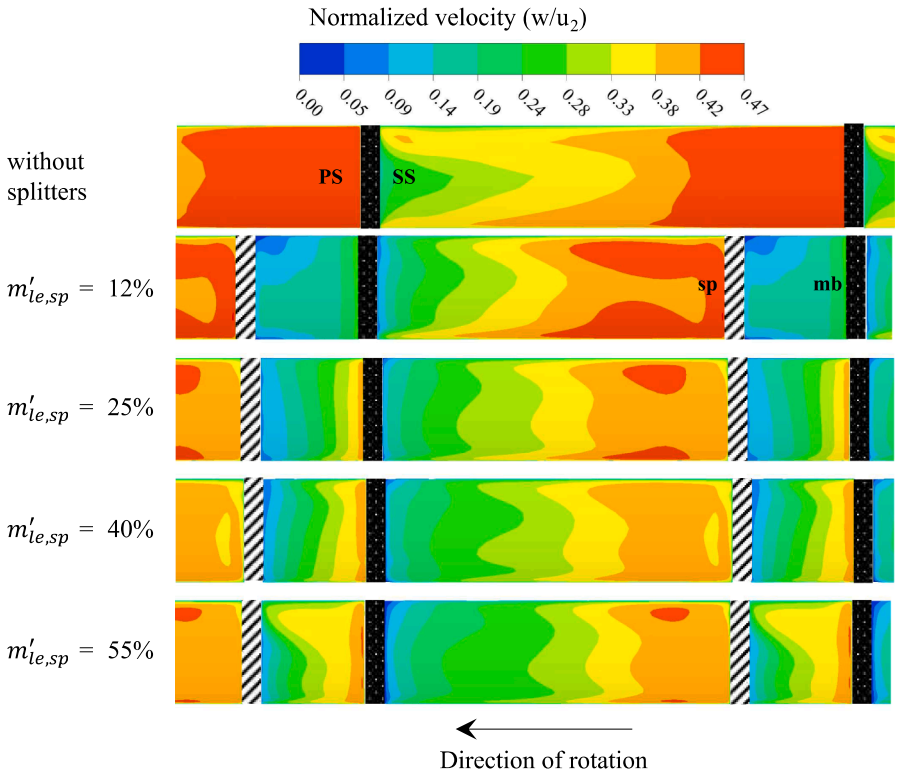

Fig. 10. Contours of normalized velocity (w/u_2) at the trailing edge for shrouded impellers (5 blades, $\beta_B = 22.5°$, $\varphi_{sp} = 25\%$, n = 50,000 rpm).

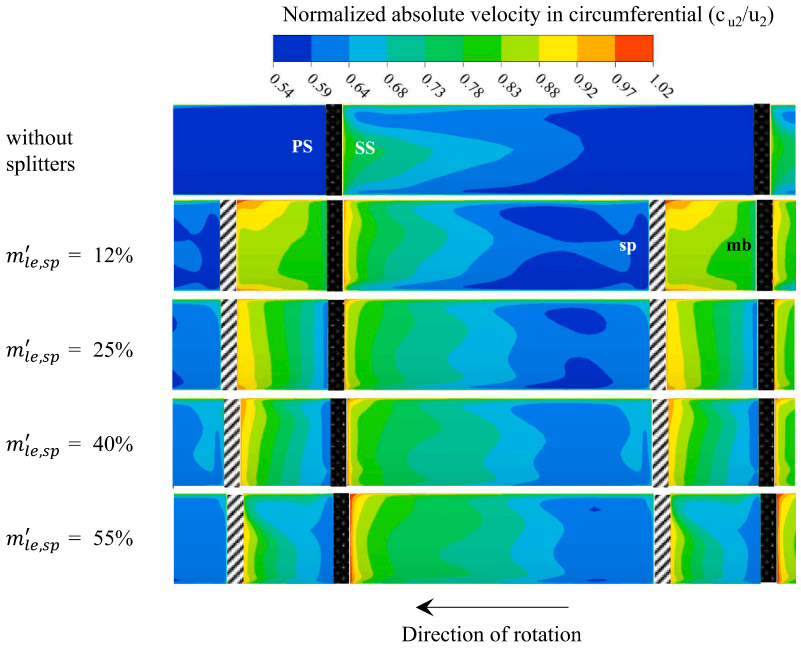

Fig. 11. Contours of normalized circumferential component of absolute velocity at the trailing edge for shrouded impellers (5 blades, $\beta_B = 22.5°$, $\varphi_{sp} = 25\%$, n = 50,000 rpm).

the splitter pitch of 0.5, where the highest head coefficient and slip factor are observed. When the splitters are placed in the middle of the adjacent main blades, the flow accelerates more than for other pitches (see Fig. 14), thus reducing the static efficiency.

Fig. 14 shows the contours of the normalized circumferential component of absolute velocity (c_{u2}/u_2) at the trailing-edge section for different placements of splitters. The contour plots imply higher velocity at the impeller outlet for a pitch value of 50%, which results in the lower static efficiency seen in Fig. 13. The figure suggests that the circumferential component of absolute velocity between the suction side of the main blade and the adjacent splitter increases with the increased pitch of splitters until it reaches a maximum at a pitch value of 50%, and then it tends to decrease as the pitch is increased further. At the same time, it decreases between the pressure side of the main blade and the adjacent

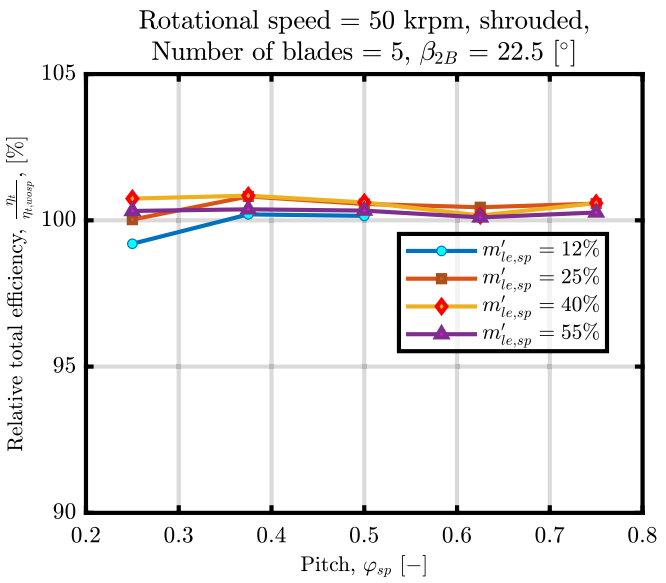

Fig. 12. The effects of pitch and length of splitter blades on the total efficiency.

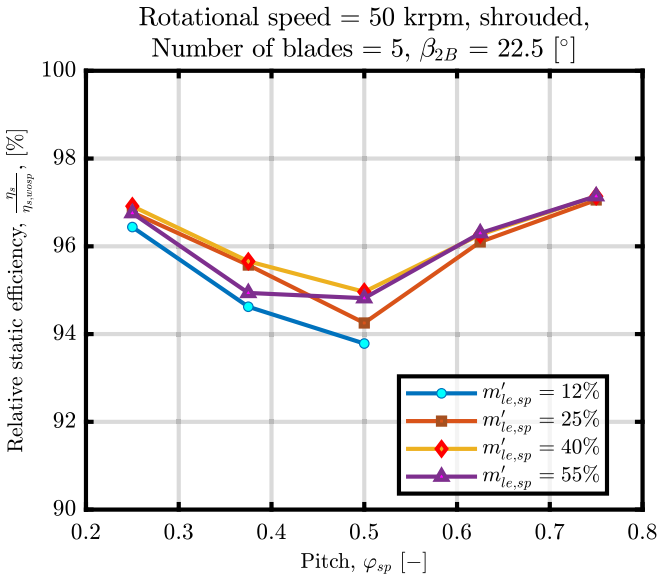

Fig. 13. The effects of pitch and length of splitter blades on the static efficiency.

splitter.

Effect of blade outlet angle

The change of relative head coefficients with splitters pitch for three blade outlet angles of 22.5°, 50°, and 90° is plotted in Fig. 15. The head coefficient for each blade outlet angle is relative to the value obtained for the same impeller without splitter blades. The same trend is observed for each blade outlet angle; the head coefficient increases initially and then decreases as the pitch of splitters increases. The figure suggests that the use of splitter blades is more pronounced for radial blades (β_{2B} = 90°) when the splitters are in the middle of the adjacent main blades (φ_{sp} = 0.5). The optimal pitch moves closer to the pressure side of the main blades for highly backswept impellers (e.g., β_{2B}=22.5°).

Fig. 16 presents the effect of blade outlet angle on the slip factor of shrouded impellers with splitters relative to the respective impellers without splitter blades. The curves suggest a more significant increase in the slip factor for impellers with a blade outlet angle of 50° compared to the blade outlet angles of 22.5° and 90°. In contrast, Fig. 15 reveals that the relative head rise of the two latter is higher. Such observation suggests that although the flow is better guided for the case ofβ_{2B} = 50°, which leads to less slip, the losses are more pronounced for such impellers with splitter blades. Consequently, a lower efficiency is expected for impellers with a blade outlet angle of 50°, which is highlighted in Fig. 17.

Fig. 17 shows the change of total efficiency for shrouded impellers with splitters for three blade outlet angles of 22.5°, 50°, and 90°. Similarly, for all blade outlet angles, the splitters have little influence on the total efficiency. For radial blades (β_{2B} = 90°), an increase of 1 % is observed for the total efficiency when the splitters are placed in the middle of the adjacent main blades. For other pitches, no perceptible improvement in total efficiency is observed.

The influence of blade outlet angle on the static efficiency for shrouded impellers is shown in Fig. 18. The figure suggests that at each blade outlet angle, the static efficiency reaches its minimum at the splitter pitch of 50 %, like the trend observed in Fig. 13. Moreover, the figure suggests that the static efficiency decreases with the increase of the blade outlet angle so that it decreases by 13 % for the blade outlet angle of 90°.

Effect of the number of blades

Fig. 19 presents the influence of the number of blades on the characteristic indicators. The values are relative to respective impellers without splitters and the reference values are given in the sub-figures. The figure suggests that the benefits of adding splitter blades decrease with the number of blades, as the head coefficient and slip factors of an impeller with 5 blades increase more than the ones of a 6-bladed impeller. Adding splitters to an impeller with a higher number of blades increases friction and shock losses, lessening the beneficial influence of splitter blades. The negative impact of increasing the number of blades on the efficiency is consistent with the results of Gölcü et al. [3] on deep-well pumps. However, contrary to the results of Gölcü et al. [3], no negative influence of splitters with 6 main blades is observed on performance, as the head coefficient, slip factor, and total efficiency are still improved by using splitter blades in impellers with 6 blades.

Effect of tip clearance

Fig. 20 shows the effect of tip clearance on the head coefficient (relative to the respective impellers without splitters) for the different pitches for impellers with radial blades. Different trends of variation of head rise with the pitch can be observed according to whether the impeller is shrouded or unshrouded. The figure suggests that the placement of the splitter in the middle of the adjacent main blades (φ = 50 %) does not necessarily lead to the maximum head coefficient for unshrouded impellers.

In Fig. 21, the slip factors are plotted as a function of the splitter blade pitch for shrouded and unshrouded impellers with radial blades. The figure suggests that the change of slip factors with the pitch is consistent with the change of the head coefficient with the pitch. However, although splitter blades increase the slip factor for the impeller with a 0.1 tip clearance ratio more significantly than for the 0.05 tip clearance ratio pump, the relative head coefficient changes are smaller for the tip clearance ratio of 0.10. Hence, although the splitter blades improve the flow guidance in the impeller passage, the secondary flow losses are suggested to increase with tip clearance penalizing the increase in head coefficient.

The contour of the non-dimensional stagnation pressure at the impeller output (defined in Eq. (22) and Eq. (23)) can be used to visualize the loss distribution with increasing tip clearance ratios. The contour is shown in Fig. 22. The figure suggests that the minimum reduced stagnation pressure decreases with increasing tip clearance ratios. In addition, the region with the lowest value is seen to grow. When the tip clearance is larger, more flow leaks through it and does not get completely mixed with the main flow. As a result, the stagnation

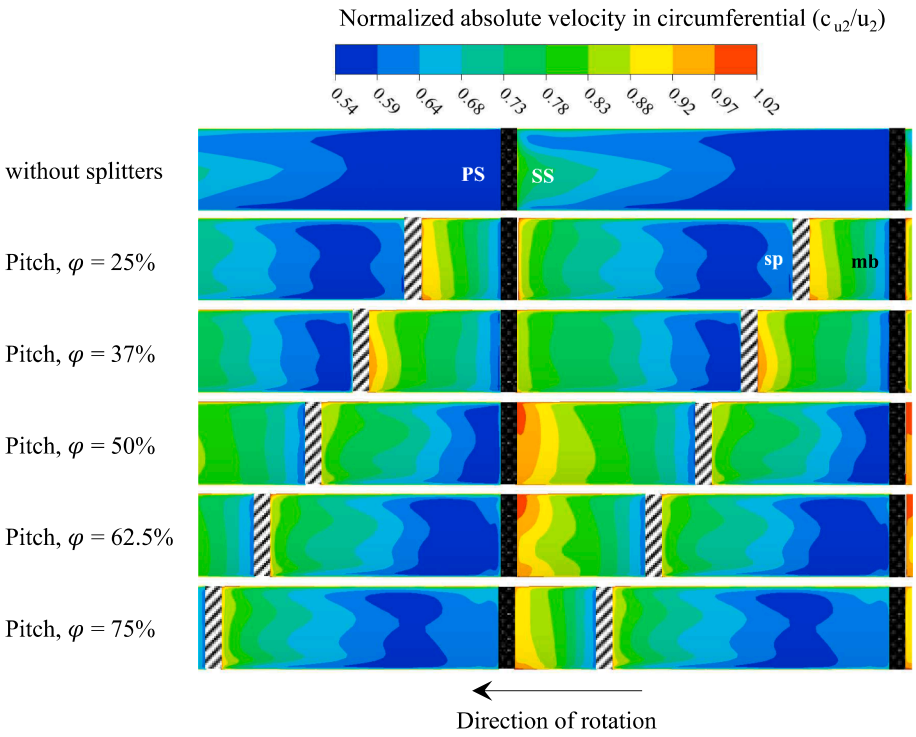

Fig. 14. Contours normalized circumferential component of absolute velocity (c_{u2}/u_2) in the impeller passage (5 blades, shrouded, $\beta_B = 22.5°$, $m'_{le,sp} = 25\%$, n = 50,000 rpm).

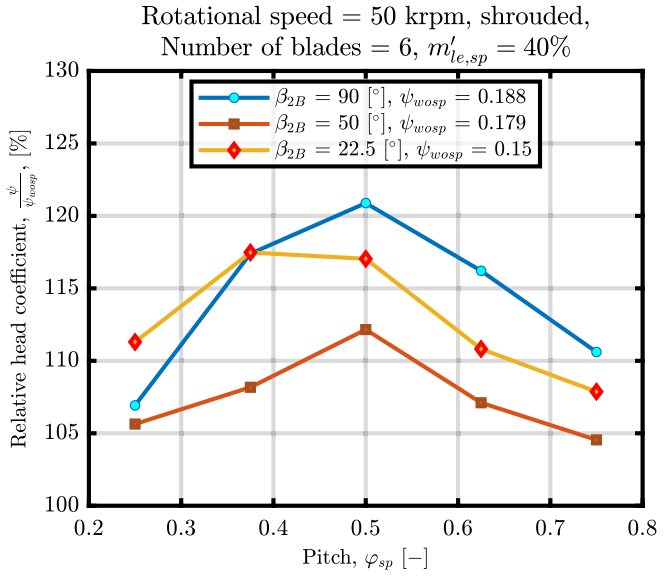

Fig. 15. The effect of blade outlet angle on the head coefficient.

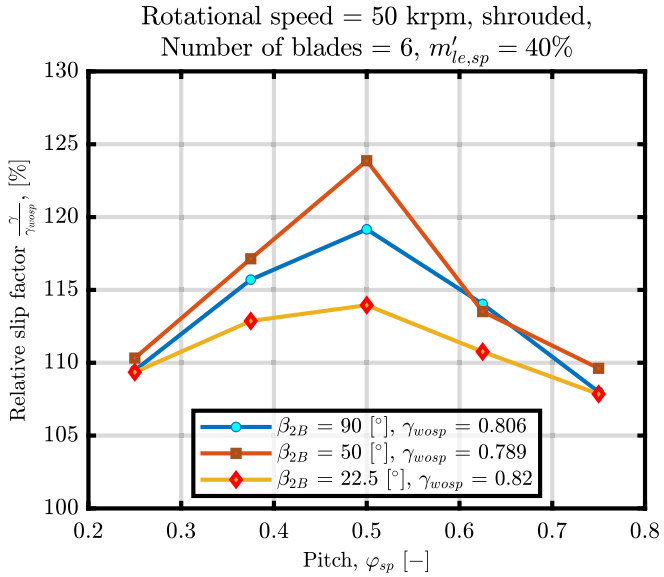

Fig. 16. The effects of blade outlet angle on the slip factor.

pressure decreases.

$$p_{T,\,red} = p_S + \frac{\rho}{2}\left(w^2 - u^2\right) \tag{22}$$

$$C_{p_{T,red}} = \frac{p_{T,\,red} - \overline{p_{T,\,red,\,in}}}{\rho u^2} \tag{23}$$

Fig. 23 shows the effect of tip clearance and splitter blade pitch on the total efficiency of impellers with radial blades. Higher total efficiency is observed when the splitter blades are employed in unshrouded impellers with a small tip clearance ratio (c/b = 0.05). In addition, when the splitters are placed in the middle of adjacent main blades, the total efficiency is not influenced by whether or not the impeller is shrouded and the tip clearance ratio.

The influence of the tip clearance ratio on the static efficiency at different splitter blade pitches for impellers with radial blades is shown in Fig. 24. The figure suggests that splitter blades' static efficiency is less affected as the tip clearance increases. The lowest ratio of static efficiency decrement is observed for the tip clearance ratio of 0.10; it decreases by 3 % compared to 13 % for shrouded impellers.

The numerical analysis and the non-extensive representation of the results above seem to suggest a strong influence of the splitter blades on the turbopump performance. Unfortunately, trends regarding the length

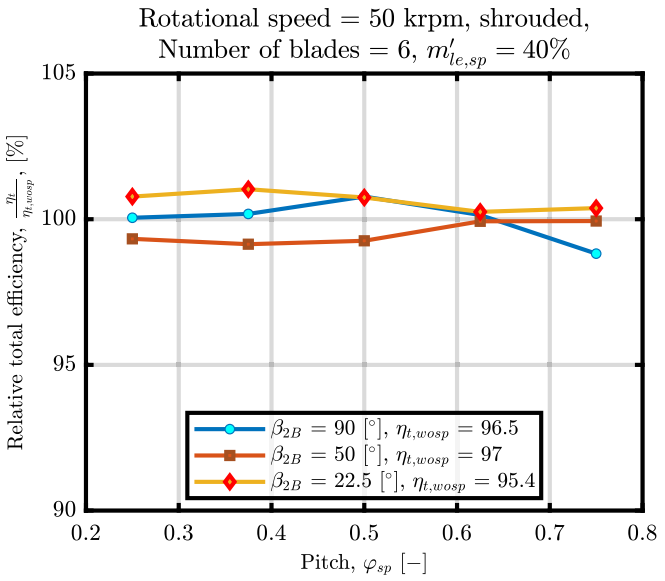

Fig. 17. The effects of blade outlet angle on the total efficiency.

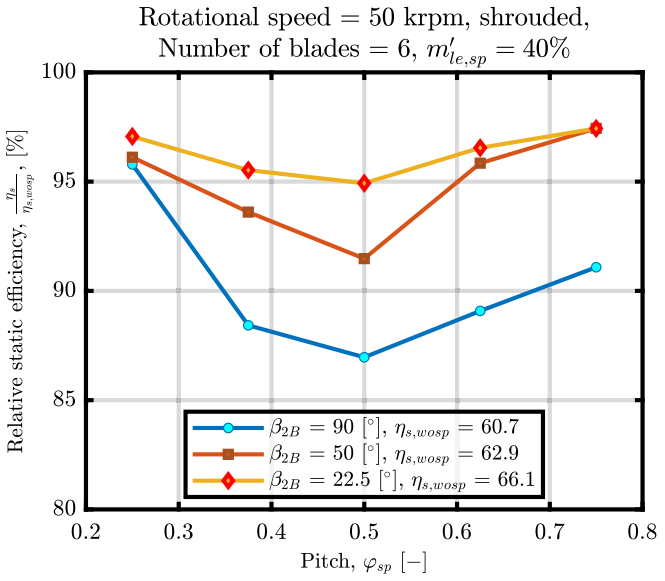

Fig. 18. The effects of blade outlet angle on the static efficiency.

and the angular position of the splitter blades for shrouded and unshrouded impellers with different tip clearances are not straightforward. Consequently, it was decided to infer a surrogate model based on neural networks using the obtained results.

Neural network model

Estimating the slip and the head rise of impellers due to the combined effects of splitter blades and tip clearance can be achieved with neural network (NN) based surrogate models. The parametric design tool enables the training of NN models on a wide range of design parameters. The NN models are trained based on the parameters and performance indicators achieved with the range of parameters listed in Table 1. 150 unshrouded impellers and their equivalent shrouded impellers are randomly generated with the Optimal-Space Filling (OSF) design technique [33]. The geometries are then solved with the CFD solver to obtain well-sampled additional performance data. The parameters and performance of these geometries are not seen by the NN models before and are used as test data, so the accuracy of the generated models can be evaluated with no bias.

The training for a selected learning algorithm continues with finding the optimal NN structure through an iterative process. In each iteration, the weights and biases of the neurons in the algorithm are adjusted by evaluating the model's performance against the training data.

The neuron is the sum of the weighted average of its input and a constant term called the bias unit. The weights determine the effect of each input on the next layer, while the bias units, independent of the previous layer, ensure that the neuron can still get activated despite a case where all inputs are zero. A non-linear function (activation function) is then applied to the sum. Therefore, the neurons of layer i can be computed as (See Fig. 25):

$$Z_i = W^{(i)}(\sigma(Z_{i-1})) + b^{(i)} = W^{(i)}h_{i-1} + b^{(i)} \tag{24}$$

Where σ is the activation function set to the previous layer and h is its output. The objective function to be minimized is the mean squared error of predicted values with the NN model from values calculated with the CFD analysis and is described as Eq. (25), where m is the number of training data.

$$J(\Theta) = \frac{1}{2m}\sum_{i=1}^{m}\left(y_{CFD}^{(i)} - y^{(i)}\right)^2 \tag{25}$$

The NN models of this research are developed with Flux [34] in the Julia programming environment [35]. Flux is an open-source NN package making efficient use of Julia's native code for gradient computation, resulting in lower computation time. The slip factor model takes the splitters' pitch and relative meridional length, the tip clearance ratio, the number of blades, and the blade outlet angle as input parameters. In addition to the input parameters of the slip model, the head coefficient model takes the flow angle at the leading edge of the main blade, the ratio of the inlet to outlet diameters, and the specific speed as input parameters.

The slip factor model predicts the slip of both shrouded and unshrouded impellers. The model of head coefficient estimates the relative head of an unshrouded impeller with splitters ($\frac{\Delta\psi}{\psi_0}$) compared to the base-shrouded impeller with splitters:

$$\frac{\Delta\psi}{\psi_0} = \frac{(\psi_0 - \psi) - (\psi_{in0} - \psi_{in})}{\psi_0} \tag{26}$$

where ψ_0 is the head coefficient of the respective shrouded impeller and ψ_{in} is the input head coefficient of the impeller. The term $(\psi_0 - \psi)$ is the apparent difference in the head coefficient between an unshrouded impeller and its respective shrouded impeller, and the term $(\psi_{in0} - \psi_{in})$ is the difference in input head coefficient between the two impellers. The input head of an impeller is calculated as follows:

$$H_{in} = \frac{U_2^2 - U_1^2 + W_1^2 - W_2^2 + C_2^2 - C_1^2}{2g} \tag{27}$$

Out of 300 hundred test impellers (shrouded and unshrouded), the CFD solutions of 267 impellers are converged successfully and used to test the slip model. For each test data for the head coefficient model, CFD solutions of the unshrouded impeller and its corresponding shrouded impeller are required. Since CFD solutions of some shrouded and unshrouded geometries do not converge, 92 test data out of 150 cases are available to evaluate the accuracy of the head coefficient model.

A feedforward neural network with two hidden layers of 7 and 4 neurons, each with a sigmoid activation function, determines the best algorithm for the slip factor. The relative deviation of slip factors predicted by the NN model for training and test data is shown in Fig. 26. The NN model predicts 100 % of both training and test CFD data within a ± 5% relative deviation, resulting in an average absolute deviation of 0.66 % for the training and 1.30 % for the test data.

The best NN scheme for the head coefficient consists of two hidden layers with 5 and 3 neurons, each with a sigmoid activation function.

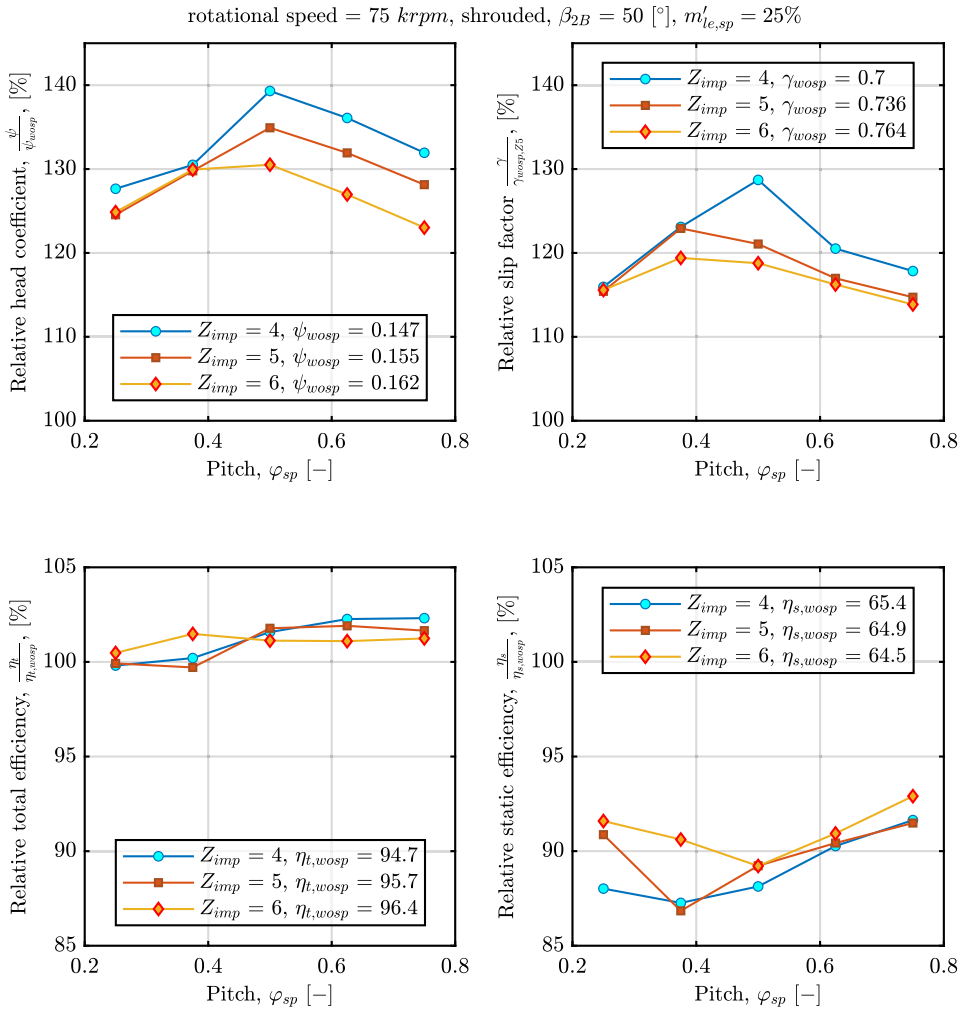

Fig. 19. The influence of the number of blades on characteristic parameters.

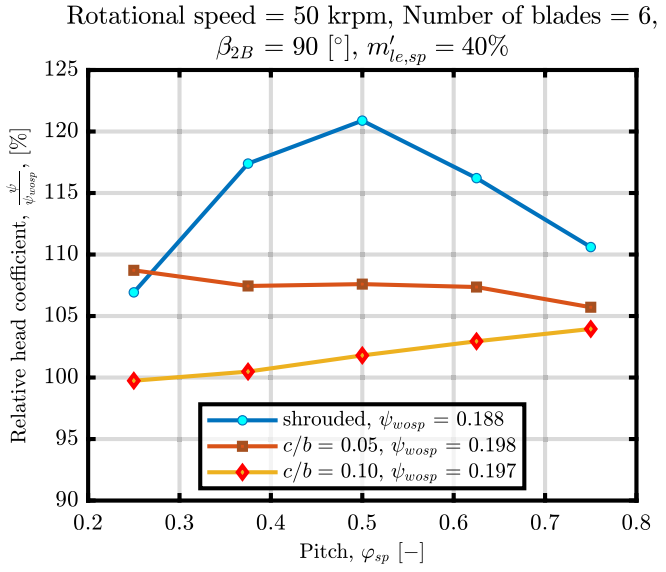

Fig. 20. The effect of tip clearance and splitter blade pitch on the head coefficient.

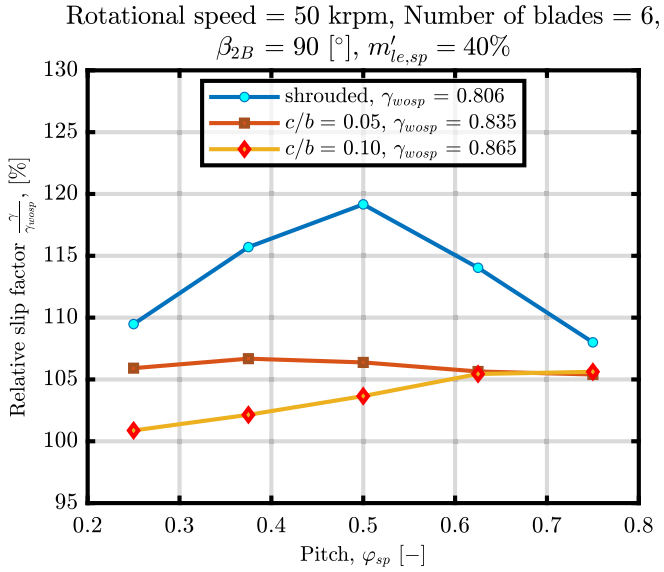

Fig. 21. The effects of tip clearance and splitter blade pitch on the slip factor.

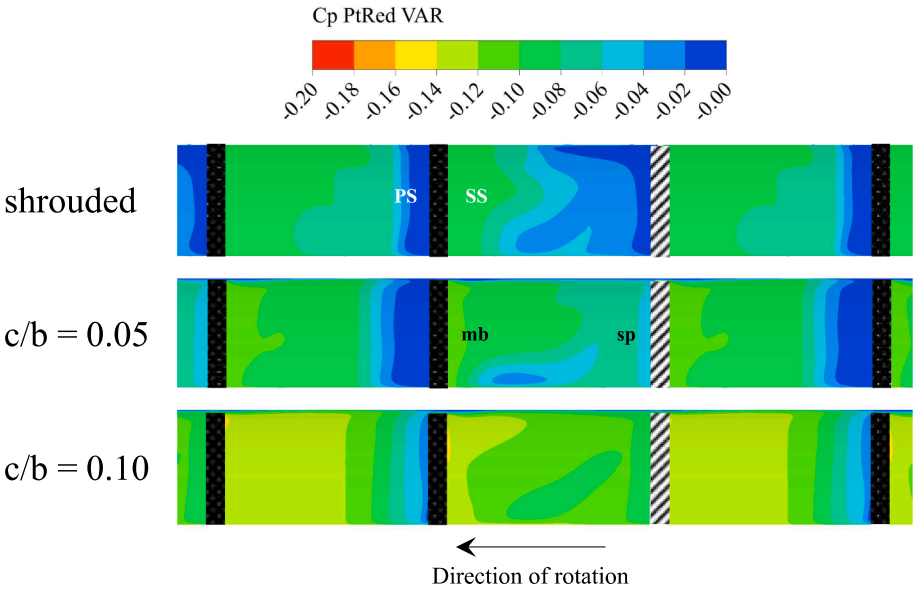

Fig. 22. Contours of non-dimensional stagnation pressure contour ($C_{P_{T,r}}$) at the impeller outlet (6 blades, shrouded, $\beta_B = 90°$, $m'_{le,sp} = 40\%$, n = 50,000 rpm).

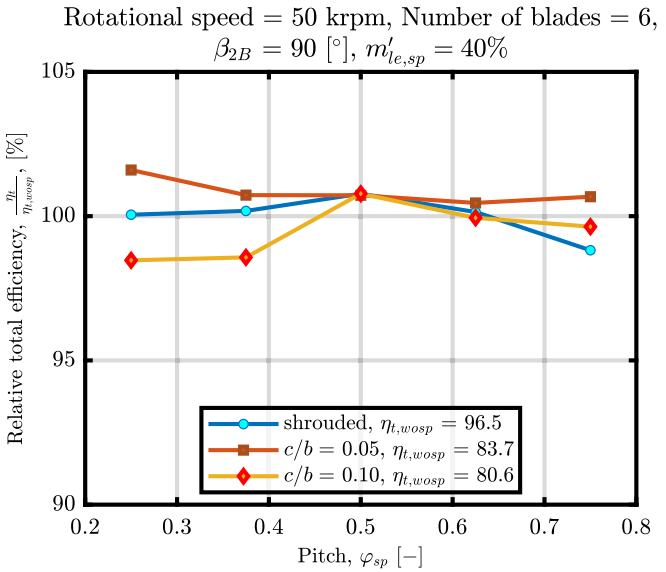

Fig. 23. The effects of tip clearance and splitter blade pitch on the total efficiency.

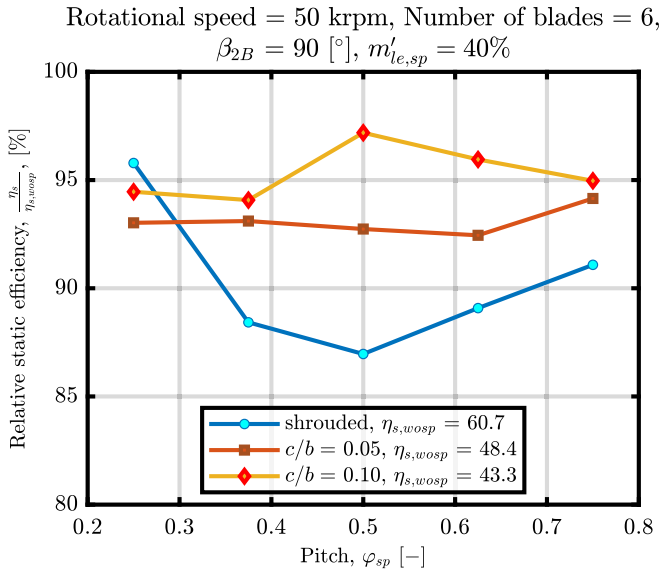

Fig. 24. The effects of tip clearance and splitter blade pitch on the static efficiency.

Fig. 27 shows the relative deviation of head loss coefficients predicted by the NN model for training and test data. The figure suggests that 100 % of CFD data are estimated within a ± 10% relative deviation with an average absolute deviation of 1.3 % for training and 5.7 % for test data.

The developed NN models appropriately translate input data into their correct values for the slip factor and head loss coefficient. The model can be used to efficiently identify the ideal spitter blade pitch and leading-edge position for any turbopump impeller within the geometry and operational values in Table 1. The parameters of the NN models predicting the slip factor and head loss coefficient are available in a data repository [36].

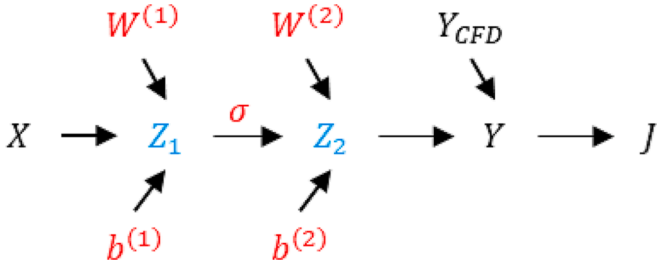

Fig. 25. General neural network architecture.

Design optimization

While the previous sections suggested that the splitter blades can improve the head rise and the slip factor, their influences are not as evident on unshrouded impellers as they are for shrouded impellers. The tip clearance impairs the performance of unshrouded impellers [26]. The results also suggested that the splitters have a minimal impact on total efficacy. Therefore, this section aims to determine whether a better design can be achieved through optimization to increase the head rise

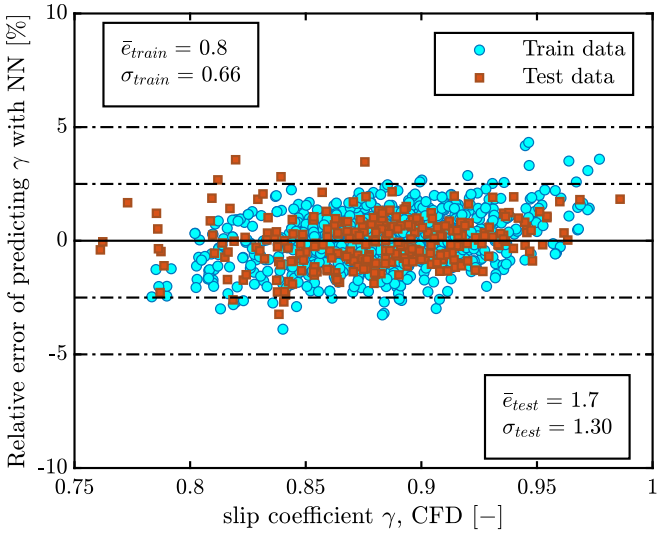

Fig. 26. Relative deviation of slip factor predicted with the NN model from CFD results.

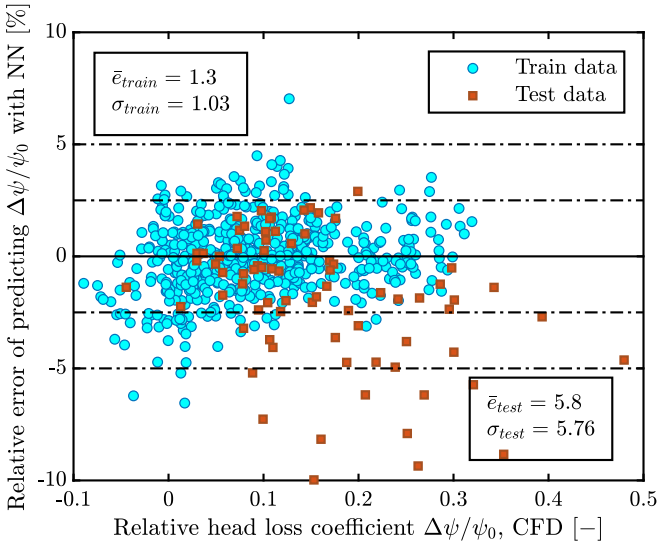

Fig. 27. Relative deviation of head coefficient predicted with the NN model from CFD results.

and efficiency while mitigating the impact of tip clearance on performance degradation.

Improvement of meridional profiles

The effect of meridional profiles of the hub and shroud on pump performance is investigated for both shrouded and unshrouded impellers with splitter blades. Two impellers with blade outlet angles of 22.5° and 90 running at 50,000 rpm are selected for the investigations. The splitter blades of both impellers are in the middle of the main blades ($\varphi_{sp} = 0.5$) and their relative leading-edge locations are at 25 %. Initially, the profiles are obtained with a linear distribution of the cross-section area ($F_1(r)$), leading to a linear change of the theoretical meridional velocity (blade blockage is not considered). Five more distributions of the cross-section area, depicted in Fig. 28, are studied to investigate the effect of meridional profiles on performance. Functions of F_2 and F_3 are parabolic (2nd-order) curves with a larger cross-section change in the vicinity of the outlet and the inlet, respectively. The Functions of F_4 and F_5 are 3rd-order polynomials. The first has a more significant cross-section change at both ends, while the latter has the greatest change in the middle.

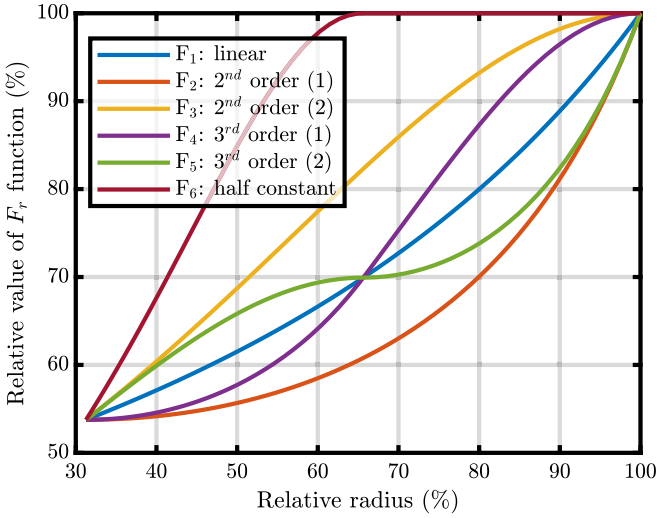

Fig. 28. Area distribution functions for generation of meridional profiles.

Finally, F_6 leads to a sharp cross-section variation at the inlet and a smooth outlet change.

Fig. 29 and Fig. 30 present the performance characteristics, including head coefficient, total efficiency, and static efficiency achieved with different distribution functions for impellers with the blade outlet angle of 22.5° and 90°, respectively. The performance characteristics are relative to characteristics achieved with the F_1 distribution function. The figures suggest that the distribution of cross-section has little effect on the performance of shrouded impellers. Zakeralhoseini and Schiffmann [26] reported extremely low hydraulic losses of shrouded impellers designed with the F_1 distribution function, leading to very high total efficiency. Thus, the gain of such iterations on the area distribution is expected to be minimal. However, by accepting a slight decrease in static efficiency, it is possible to achieve higher head coefficients up to 1.9 % for the blade outlet angle of 22.5° and 4.5 % for the blade outlet angle of 90°.

For unshrouded impellers, the figures suggest that the distributions with a greater change of cross-section area in the inlet region lead to higher performance characteristics. As much as a 4 % increase in the head coefficient and total efficiency and an 8 % increase in the static efficiency can be achieved with the F_6 distribution function for the tip clearance ratio of 0.10. The F_6 distribution function improves the characteristics of the impeller with a tip clearance ratio of 0.05 so that more than a 5 % increase in static efficiency can be achieved. Higher static efficiency of the impeller is likely to lead to lower losses in downstream components, e.g., diffusers and volutes, since the flow velocity at the outlet of the impeller will be smaller, and the friction loss is proportional to the square of the velocity.

Fig. 31 compares the meridional profiles achieved with the F_6 distribution function to those achieved with the initial F_1 distribution function.

Fig. 32 compares the contours of normalized velocity (w/u_2) obtained with the F_1 and F_6 distribution functions for the impeller with a tip clearance ratio of 0.10. A lower velocity magnitude at the shroud tip suggests that the tip leakage flow and its influence on the main flow can be reduced for the design achieved with the F_6 distribution. The visualization of streamlines can help clarify the influence of tip-leakage flow on the main flow. Fig. 33 presents the streamlines, colored by relative velocity (w/u_2), and the contours of total pressure. The figure suggests the wake region between the pressure surface of the main blade and the splitter blade for the impeller designed with the F_1 distribution (left) vanishes for the impeller designed with the F_6 distribution (right). Although the wake region remains between the suction surface of the main blade and the splitter blades, the energy imparted to the flow is

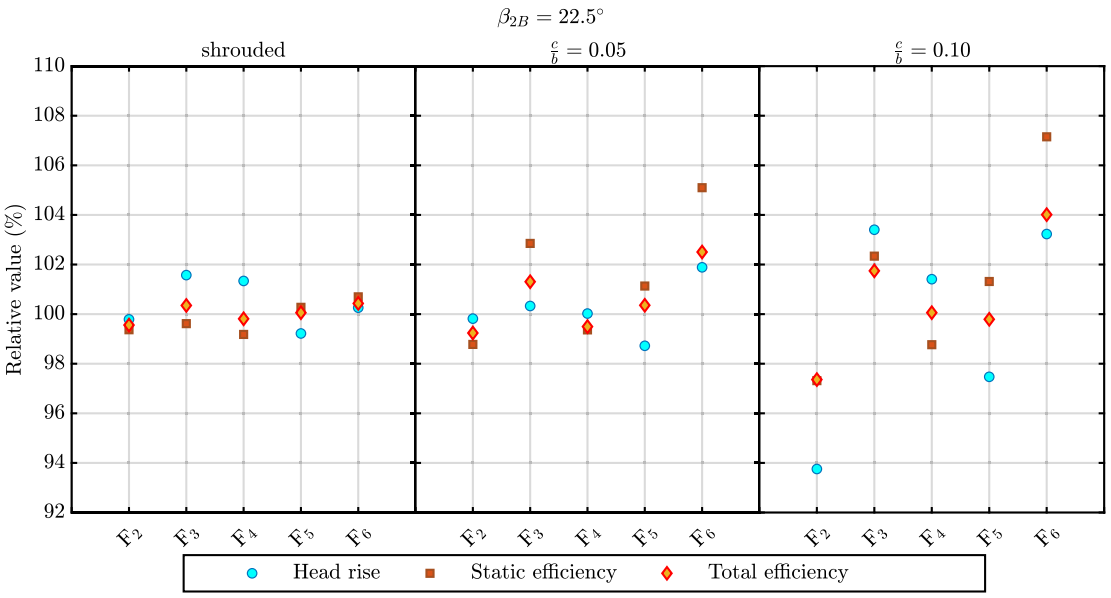

Fig. 29. The effect of area distribution functions on the head rise, static efficiency, and total efficiency normalized by the performance obtained by the linear distribution (F_1).

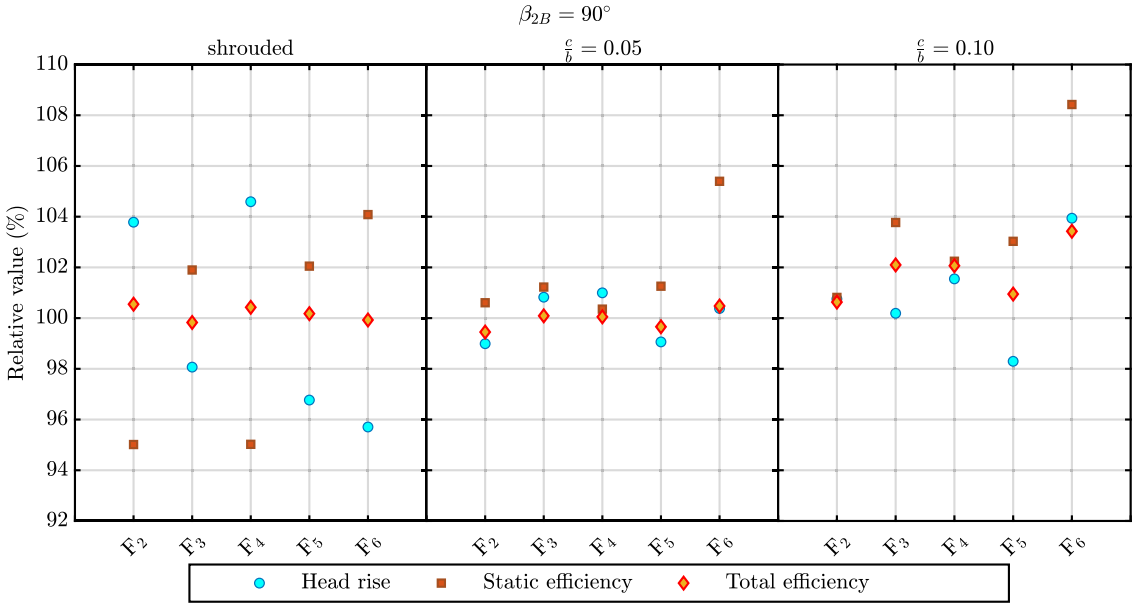

Fig. 30. The effect of area distribution functions on the head rise, static efficiency, and total efficiency normalized by the performance obtained by the linear distribution (F_1).

improved as the secondary losses caused by the tip clearance diminish. Fig. 34.

Improvement of splitter blade profiles

It is observed that the influence of tip clearance on the performance of unshrouded impellers can be mitigated by employing splitter blades and modifying the meridional profiles of the hub and shroud. In the next step, the profile of the splitter blades can be modified (depart from the main blade geometry) to study its influence on the performance and possible mitigation of tip clearance effects. For this purpose, the development of the splitter blade angle (β) is uncoupled from the main blade. It is defined separately as a parabolic distribution from the leading edge to the trailing edge of the splitter blades as follows:

$$\beta_m = (\beta_{le,sp} - \beta_2)m^2 + 2(\beta_2 - \beta_{le,sp})m + \beta_{le,sp} \quad (28)$$

The β-angle function is defined in such a way that the function's extremum is placed at the blade trailing edge to minimize the flow variation in the vicinity of the outlet. While the splitters' pitch and their leading edge's location remain constant, the leading-edge angle varies between 15° to 40°.

The elliptic profile of the splitter blades is also changed to study its influence in improving the flow characteristics in the vicinity of the leading edge. The elliptical shape can be controlled with the ratio of the semi-major axis (a) to the semi-minor axis (b), which is called the ellipse ratio (Fig. 4). The blade thickness constrains the semi-minor axis (b); therefore, the ellipse ratio is changed by changing the semi-major axis of the elliptic profile.

The design space is constructed with the OSF design technique. The OSF design technique, an optimized Latin Hypercube Sampling (LHS),

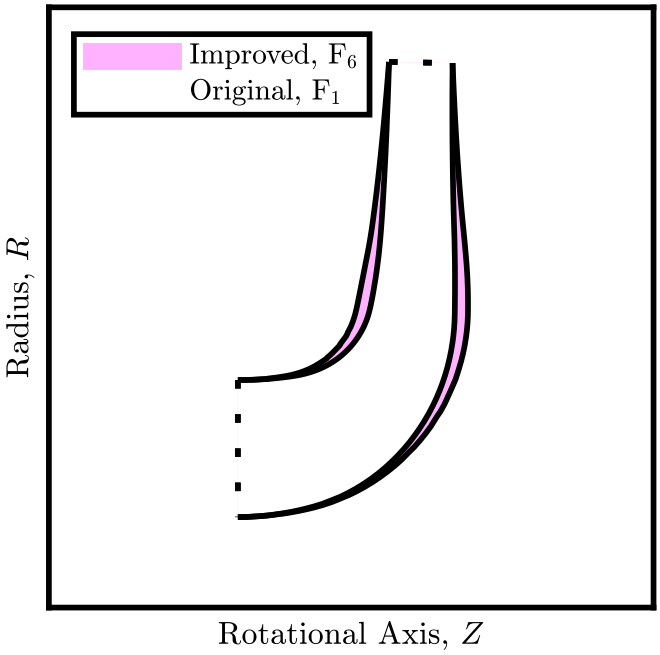

Fig. 31. Meridional profiles obtained with F_6 distribution compared to F_1 distribution.

reduces the number of design points to best cover the design space. The optimization is carried out for a shrouded impeller and two unshrouded impellers with tip clearance ratios of 0.05 and 0.10. All other impeller parameters are the same, each with a blade outlet angle of 22.5°. For each sample point generated by the OSF sampling technique, the parametric design tool generates the geometry and performs the CFD analysis through the framework of ANSYS Workbench. Once the analysis is carried out, the results are processed and saved in an ASCII-text file, which the parametric design tool then interprets. The head coefficient and total efficiency will be simultaneously maximized for the splitter leading edge angle ($\beta_{le,sp}$) and the ellipse ratio (ϵ). Thus, the objective functions and boundaries of the optimization problem are defined as follows:

$$\text{Maximize } \eta_t = f_\eta(\beta_{le,sp}, \epsilon) \tag{29}$$

$$\text{Maximize } \psi = f_\psi(\beta_{le,sp}, \epsilon)$$

$$\text{Subject to } 1 \leq \epsilon \leq 25$$

$$15^\circ \leq \beta_{le,sp} \leq 40^\circ$$

Once the costly objective function is evaluated at sample points, the algorithm builds a response surface. It then uses the generated response surface to predict the objective functions in the entire design space. The response surface is updated throughout the optimization as the algorithm will search for a new different sample point for the subsequent costly function evaluation and reconstruct the response surface. The Non-Dominated Sorting Genetic Algorithm II (NSGA-II) [37] is employed in a multi-objective optimization problem to search in the response surface to find the optimal geometry of the splitter blades.

Table 2 compares the optimized impellers' design variables and performance characteristics with the baseline designs. The lower leading-edge angle of the optimized solutions compared to the baseline designs suggest that the position of the leading edge moves toward the suction side of the main blades (see Fig. 35).

Fig. 35 shows the optimized splitters compared to the baseline splitters. The optimized splitters are longer than the baseline, suggesting higher friction loss, while the total efficiency is increased for the optimized splitters. Such an increase suggests a reduction in hydraulic losses compared to the baseline splitters.

The improved performance of the optimized splitter can be explained by Fig. 36, which compares the contours of normalized velocity (w/u_2) at the mid-span between the baseline design and optimized design for the shrouded impeller. The figure suggests that the wake region (blue contours) between the suction side of the main blade and the splitter is moderated by optimizing the splitter blades. In addition, the flow is accelerated significantly along the pressure side of the splitters (red contours) for the baseline design. The optimized splitter blades diminish the negative influence of the splitters on the approaching flow, inducing a less severe pressure gradient around the leading edge of the splitters. The finding is consistent with the conclusion made by Zhou et al. [5] that the leading edge of splitter blades considerably affects performance.

Conclusions

The performance of shrouded and unshrouded impellers suitable for small-scale ORCs is studied numerically using CFD analysis to determine the influence of adding splitter blades. A parametric design tool is developed to generate different turbopump geometries that can be examined through CFD analyses. The analysis is carried out on 1620 impellers with different design parameters, and the influence of the parameters on the performance characteristics is established. Engineers

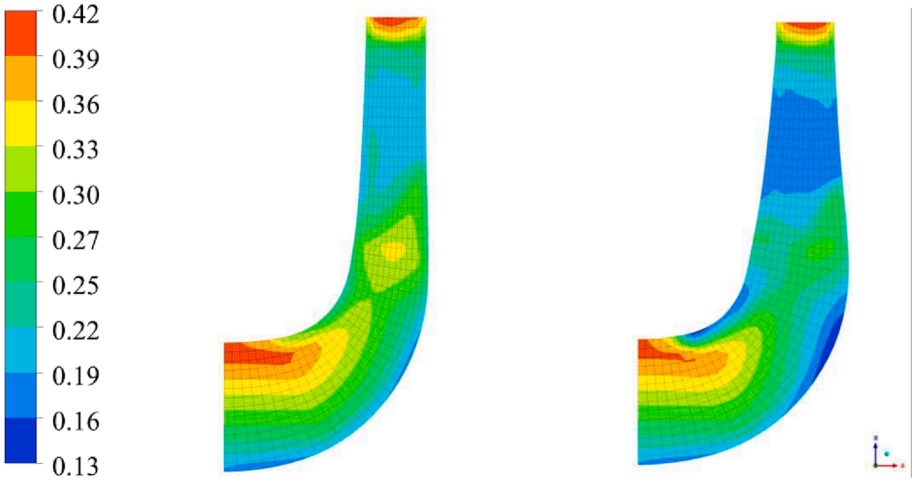

Fig. 32. Meridional contours of normalized velocity (w/u2) for profiles obtained with the F_6 distribution (right) compared to profiles obtained with the F_1 distribution (left).

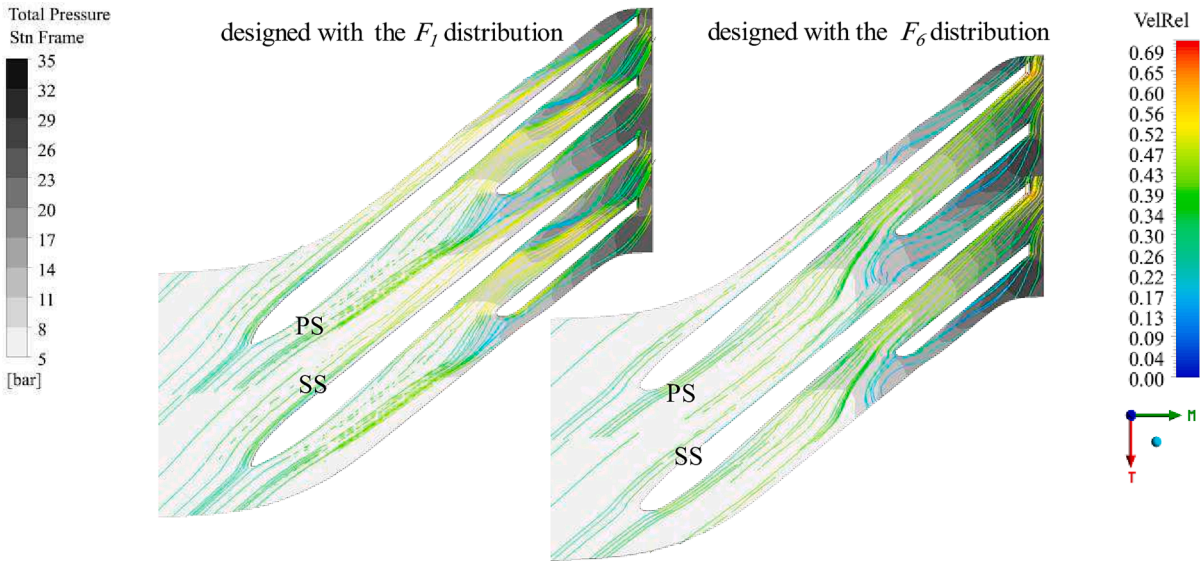

Fig. 33. Streamlines and contours of total pressure for profiles obtained with the F_6 distribution (left) compared to profiles obtained with the F_1 distribution (right).

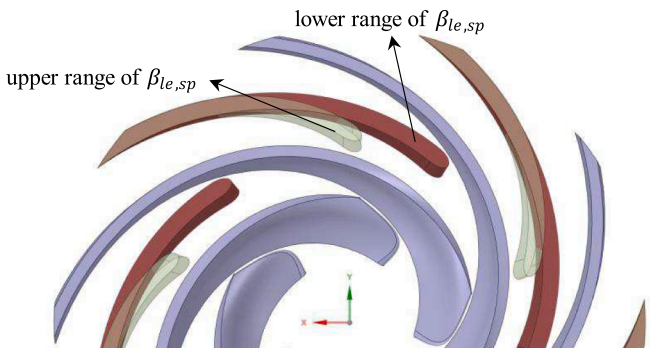

Fig. 34. Splitter blades generated with the upper and lower range of $\beta_{le,sp}$.

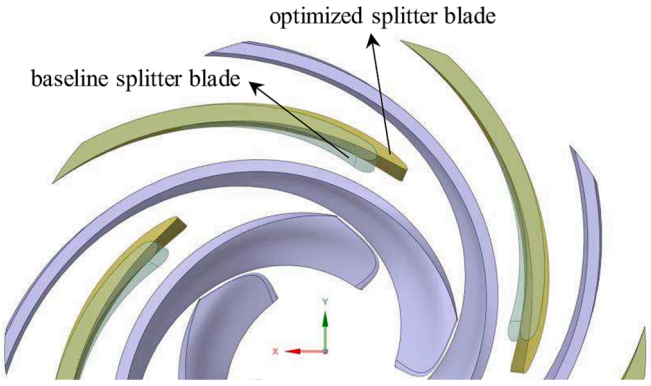

Fig. 35. Comparison of the optimized profile with the baseline design for the shrouded impeller.

Table 2
Optimization of blade profile.

Variable		shrouded	c/b = 0.05	c/b = 0.10	Unit
Blade angle at LE	Initial	26.35	26.35	26.35	(°)
	Optimized	19.15	21.5	21.3	(°)
Ellipse ratio at LE	Initial	2	2	2	(–)
	Optimized	14	18	18	(–)
Head rise		0.74	0.48	0.01	Relative increase (%)
Total efficiency		1.42	0.10	2.43	Relative increase (%)
Static efficiency		0.97	1.14	−0.49	Relative increase (%)

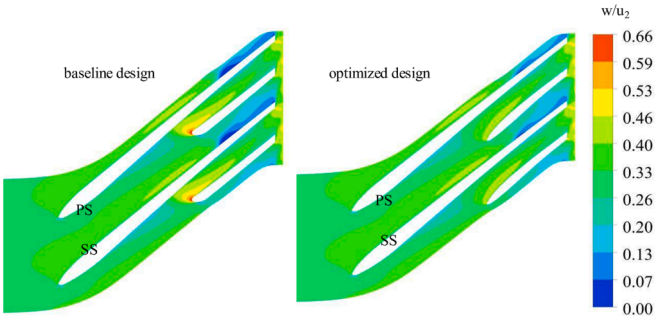

Fig. 36. Comparison of contours of normalized velocity (w/u_2) at the mid-span between the baseline design (left) and optimized design (right).

may design small-scale turbopumps with fewer iterations using the reduced-order models given in this study. The CFD results are utilized to infer different surrogate and reduced-order models to predict the performance characteristics, including slip factor and head coefficient. The models can be applied to predict the influence of splitter blades on the performance characteristics of centrifugal turbopumps as long as the parameters in Table 1 are met. The following conclusions are drawn from the findings:

1. Splitter blades can increase the head coefficient and slip factors of impellers up to 10% – 24% depending on the blade outlet angle, the number of blades, and the tip clearance ratio.
2. While the total efficiency is not influenced significantly, the occupation of flow passage by splitter blades can decrease the static efficiency by 13 %.
3. The CFD calculations predict that the placement of splitters leading to the maximum head coefficient moves from the middle of the

adjacent main blades for shrouded impellers to the suction side of the main blade for unshrouded impellers.

4. Although the splitter blades improve the flow guidance in the impeller passage, the secondary flow losses increase with the tip clearance and penalize the increased head coefficient.
5. The influence of dominating parameters on the slip factor and the head coefficient is modeled using feedforward neural networks. The models can be used to estimate the combined effects of splitter blades and tip clearance on centrifugal turbopumps' performance. Surrogate models predict CFD data with an average relative variance of 1.7 % for the slip factor and 5.8 % for the head loss coefficient of unshrouded impellers.
6. Meridional profiles with a larger change in cross-section area near the inlet compared to a linear change are more advantageous for unshrouded impellers. Higher head rise, total efficiency, and static efficiency are observed for this new cross-section profile.
7. The optimization of splitter blade profiles is less successful than the optimization of meridional profiles in mitigating the effects of tip clearance flow, as only a 2.43 % improvement in total efficiency is achieved. In comparison, the head rise remains constant, and static efficiency decreases by 0.49 % for an impeller with a tip clearance ratio of 0.10.

CRediT authorship contribution statement

Sajjad Zakeralhoseini: Visualization, Methodology, Software, Validation, Formal analysis, Investigation, Writing – original draft. **Jürg Schiffmann:** Supervision, Project administration, Resources, Writing – review & editing.

Declaration of Competing Interest

The authors declare that they have no known competing financial interests or personal relationships that could have appeared to influence the work reported in this paper.

Data availability

Models and data are accessible through the research repository whose address can be found in the article.

References

[1] S. Quoilin, M. van den Broek, S. Declaye, P. Dewallef, V. Lemort, Techno-economic survey of organic rankine cycle (ORC) systems, Renew. Sustain. Energy Rev. (2013), https://doi.org/10.1016/j.rser.2013.01.028.

[2] K. Rahbar, S. Mahmoud, R.K. Al-Dadah, N. Moazami, S.A. Mirhadizadeh, Review of organic Rankine cycle for small-scale applications, Energ. Conver. Manage. (2017), https://doi.org/10.1016/j.enconman.2016.12.023.

[3] M. Gölcü, Y. Pancar, Y. Sekmen, Energy saving in a deep well pump with splitter blade, Energy Convers Manag 47 (5) (2006) 638–651, https://doi.org/10.1016/j.enconman.2005.05.001.

[4] G. Kergourlay, M. Younsi, F. Bakir, R. Rey, Influence of splitter blades on the flow field of a centrifugal pump: test-analysis comparison, Int. J. Rotating Mach. 2007 (2007), https://doi.org/10.1155/2007/85024.

[5] X. Zhou, Y. X. Zhang, Z. L. Ji, L. Chen, Hydraulic design and performance analysis of low specific speed centrifugal pump, in: *IOP Conference Series: Earth and Environmental Science*, 2012, vol. 15, no. PART 3. 10.1088/1755-1315/15/3/032023.

[6] T. Shigemitsu, J. Fukutomi, K. Kaji, T. Wada, Performance and internal flow condition of mini centrifugal pump with splitter blades, in: *IOP Conf. Series: Earth Environ. Sci.*, 2012, vol. 15, no. PART 7. 10.1088/1755-1315/15/7/072001.

[7] G. Cavazzini, G. Pavesi, A. Santolin, G. Ardizzon, R. Lorenzi, Using splitter blades to improve suction performance of centrifugal impeller pumps, Proc. Instit. Mech. Eng., Part A: J. Power Energy 229 (3) (2015) 309–323, https://doi.org/10.1177/0957650914563364.

[8] W. Yang, R. Xiao, F. Wang, Y. Wu, Influence of splitter blades on the cavitation performance of a double suction centrifugal pump, Adv. Mech. Eng. 2014 (2014), https://doi.org/10.1155/2014/963197.

[9] Y. Yuan, S. Yuan, Analyzing the effects of splitter blade on the performance characteristics for a high-speed centrifugal pump, Adv. Mech. Eng. 9 (12) (2017), https://doi.org/10.1177/1687814017745251.

[10] J. Zhang, G. Li, J. Mao, S. Yuan, Y. Qu, J. Jia, Effects of the outlet position of splitter blade on the flow characteristics in low-specific-speed centrifugal pump, Adv. Mech. Eng. 10 (7) (2018), https://doi.org/10.1177/1687814018789525.

[11] S. Yuan, J. Zhang, Y. Tang, J. Yuan, Y. Fu, Research on the Design Method of the Centrifugal Pump With Splitter Blades, in: *Proceedings of the ASME Fluids Engineering Division Summer Conference 2009, FEDSM2009*, Jul. 2009, vol. 1. 10.1115/FEDSM2009-78101.

[12] B. Djebedjian, Theoretical model to predict the performance of centrifugal pump equipped with splitter blades, *Mansoura Eng. J.*, 34, p. M. 50 – M. 70, 2009, 10.21608/bfemu.2020.126166.

[13] F.J. Wiesner, A review of slip factors for centrifugal impellers, J. Eng. Gas Turbine Power (1967), https://doi.org/10.1115/1.3616734.

[14] J. Zhang, S. Yuan, Y. Shen, W. Zhang, Performance prediction for a centrifugal pump with splitter blades based on BP artificial neural network, Commun. Comp. Inf. Sci. 98 (2010), https://doi.org/10.1007/978-3-642-15859-9_31.

[15] L. Ye, S. Yuan, J. Zhang, Y. Yuan, Effects of splitter blades on the unsteady flow of a centrifugal pump, Fluids Eng. Divis. Summer Meeting 44755 (2012) 435–441.

[16] M.H. Siddique, A. Samad, S. Hossain, Centrifugal pump performance enhancement: Effect of splitter blade and optimization, Proc. Instit. Mech. Eng., Part A: J. Power Energy 236 (2) (2022) 391–402, https://doi.org/10.1177/09576509211037407.

[17] H. Safikhani, A. Khalkhali, M. Farajpoor, Pareto Based Multi-Objective Optimization of Centrifugal Pumps Using CFD, Neural Networks and Genetic Algorithms, *http://www.tandfonline.com/action/authorSubmission?journalCode=tcfm20&page=instructions*, vol. 5, no. 1, pp. 37–48, 2014, 10.1080/19942060.2011.11015351.

[18] Y. Lian, M.S. Liou, Multi-objective optimization of transonic compressor blade using evolutionary algorithm, J. Propuls. Power 21 (6) (2005) 979–987, https://doi.org/10.2514/1.14667.

[19] S. Kim, Y.-S. Choi, K.-Y. Lee, J.-H. Kim, Design optimization of mixed-flow pump in a fixed meridional shape, Int. J. Fluid Mach. Syst. 4 (1) (2011) 14–24, https://doi.org/10.5293/IJFMS.2011.4.1.014.

[20] R.F. Huang *et al.*, Multi-objective optimization of a mixed-flow pump impeller using modified NSGA-II algorithm, *Sci. China Technol. Sci.* 58 (12), pp. 2122–2130, 2015, 10.1007/S11431-015-5865-5.

[21] J. Pei, W. Wang, S. Yuan, Multi-point optimization on meridional shape of a centrifugal pump impeller for performance improvement, *J. Mech. Sci. Technol.* 30 (11), 4949–4960, 2016, 10.1007/S12206-016-1015-7.

[22] J. Pei, T. Yin, S. Yuan, W. Wang, J. Wang, Cavitation optimization for a centrifugal pump impeller by using orthogonal design of experiment, Chinese J. Mech. Eng. (English Edition) 30 (1) (2017) 103–109, https://doi.org/10.3901/CJME.2016.1024.125/METRICS.

[23] J. W. Suh, J. W. Kim, Y. S. Choi, J. H. Kim, W. G. Joo, K. Y. Lee, Multi-objective optimization of the hydrodynamic performance of the second stage of a multi-phase pump, *Energies 2017, 10, 1334,* 10.3390/EN10091334.

[24] M. Namazizadeh, M. T. Gevari, M. Mojaddam, M. Vajdi, Optimization of the splitter biade configuration and geometry of a centrifugai pump impeller using design of experiment, *J. Appl. Fluid Mech.*, 13 (1), 89–10, 2020, 10.29252/jafm.13.01.29856.

[25] S. Zakeralhoseini, J. A. Schiffmann, The effects of the tip clearance on the performance of small-scale turbopumps for ORC applications; analysis and modeling, in: *Proceedings of the 6th International Seminar on ORC Power Systems*, 2021, vol. 2021, no. 112. [Online]. Available: http://infoscience.epfl.ch/record/289985.

[26] S. Zakeralhoseini, J. Schiffmann, Analysis and modeling of the tip leakage flow on the performance of small-scale turbopumps for ORC applications, Appl. Therm. Eng. (2022), 119160, https://doi.org/10.1016/j.applthermaleng.2022.119160.

[27] H.I. Choi, S.W. Choi, H.P. Moon, Mathematical theory of medial axis transform, Pac. J. Math. 181 (1) (1997) 57–88.

[28] Y. Wang, Q. Dong, Y. Zhang, Meridional shape design and the internal flow investigation of centrifugal impeller, Proc. Inst. Mech. Eng. C J. Mech. Eng. Sci. 231 (23) (2017) 4319–4330, https://doi.org/10.1177/0954406216667407.

[29] K. Rosset, V. Mounier, E. Guenat, J. Schiffmann, Multi-objective optimization of turbo-ORC systems for waste heat recovery on passenger car engines, Energy (2018), https://doi.org/10.1016/j.energy.2018.06.193.

[30] K. Rosset, O. Pajot, J. Schiffmann, Experimental investigation of a small-scale organic rankine cycle turbo-generator supported on gas-lubricated bearings, J. Eng. Gas Turbine Power 143 (5) (2021) 1015, https://doi.org/10.1115/1.4049988.

[31] ANSYS Turbogrid User's Guide. Mar. 2021.

[32] A. Nourbakhsh, A. Jaumotte, C. Hirsch, H.B. Parizi, Turbopumps and Pumping Systems, Springer Science & Business Media, 2007.

[33] P. Z. G. Qian, M. Ai, C. F. J. Wu, Construction of nested space-filling designs, *https://doi.org/10.1214/09-AOS690*, vol. 37, no. 6A, pp. 3616–3643, Dec. 2009, 10.1214/09-AOS690.

[34] M. Innes, Flux: Elegant Machine Learning with Julia, *J. Open Source Softw.*, 2018, 10.21105/joss.00602.

[35] J. Bezanson, S. Karpinski, V.B. Shah, A. Edelman, Julia: A fast dynamic language for technical computing, *arXiv preprint arXiv:1209.5145*, 2012.

[36] S. Zakeralhoseini, J. Schiffmann, Neural Network Models for Centrifugal Pumps, Mendely Data, 2022.

[37] K. Deb, A. Pratap, … S. A.-I. transactions on, and undefined 2002, A fast and elitist multiobjective genetic algorithm: NSGA-II, *ieeexplore.ieee.org*, Accessed: Aug. 12, 2022. [Online]. Available: https://ieeexplore.ieee.org/abstract/document/996017/.

[38] F. Menter, M. Kuntz, R.B. Langtry, Ten years of industrial experience with the SST turbulence model, Heat Mass Transf. 4 (2003).

[39] T. von Backström, A unified correlation for slip factor in centrifugal impellers, J. Turbomach.-T ASME 128 (2006), https://doi.org/10.1115/1.2101853.
[40] A. Stodola, Steam and gas turbines: with a supplement on the prospects of the thermal prime mover, 2, McGraw-Hill, 1927.
[41] J.D. Stanitz, Some theoretical aerodynamic investigations of impellers in radial and mixed flow centrifugal compressors, Trans. ASME 74 (4) (1952) 473–497.
[42] J. Zou, P. Wang, X. Ruan, X. Fu, A statistical method on meridional profiles of centrifugal pumps, J. Fluids Eng. 134 (2) (2012) 024502, https://doi.org/10.1115/1.4005667.